# 1

# The pseudoparticle approach to strongly correlated electron systems

Raymond Frésard[1], Johann Kroha[2], and Peter Wölfle[3]

[1] Laboratoire CRISMAT, UMR CNRS-ENSICAEN(ISMRA) 6508, and IRMA, FR3095, 6, Bld. Maréchal Juin, 14050 Caen Cedex 4, France
Raymond.Fresard@ensicaen.fr
[2] Physikalisches Institut, Universität Bonn, 53115 Bonn, Germany
kroha@physik.uni-bonn.de
[3] Institut für Theorie der Kondensierten Materie and Institut für Nanotechnologie, Karlsruher Institut für Technologie (KIT), 76049 Karlsruhe, Germany peter.woelfle@kit.edu

**Abstract.** The most prominent pseudoparticle representations and their applications to correlated spin and electronic models are reviewed, with approximate solution schemes ranging from saddle-point approximations with Gaussian fluctuations to conserving approximations and renormalization group (RG) techniques. Merits and shortcomings of these methods are described. In particular, the generic feature of radial slave boson fields to possess a finite expectation value is discussed, while pure fluctuation fields may best be treated by conserving appriximations. We present applications to the magnetic phases of the Anderson lattice model and to the Hubbard model. The non-crossing approximation and the conserving T-matrix approximation are presented and discussed as the most important conserving approximations. Furthermore RG techniques for pseudoparticle representations, including "poor man's scaling" and functional RG for the Kondo model in and out of euilibrium, a novel RG approach to the Kondo model for strong coupling, and the functional RG approach to frustrated Heisenberg models are discussed.

## 1.1 Introduction

The immense and steadily increasing field of strongly correlated electrons has emerged as a central theme of many-body physics over the past three decades (for a review see [1]). Of particular interest are the so-called heavy-fermion metallic compounds [2] and copper-oxide superconductors [3]. While fully accounting for their properties remains a challenging task, it is believed that their key properties are embodied in the Anderson or Kondo lattice models in the former case, and in the Hubbard model and the t-J-model in the latter one. The difficulty in solving these models is rooted in the fact that conventional many-body perturbation theory (including infinite resummations), does not work in these cases. This failure is obvious in lattice models with on-site repulsion $U$ exceeding the band width $D$.

Take the Hubbard model with large on-site repulsion $U$, where each lattice site can either be empty (state $|0\rangle$), singly occupied ($|\uparrow\rangle, |\downarrow\rangle$) or doubly occupied ($|2\rangle$). The dynamics of an electron will be very different according to whether it resides on a singly or doubly occupied site. For large $U$ the doubly occupied states will be pushed far up in energy, and will not contribute to the low energy physics. This leads effectively to a projection of Hilbert space onto a subspace devoid of doubly occupied states. It turns out to be difficult to effect the projection within conventional many-body theory, as has been realized early on in the context of the magnetic impurity problem. Indeed, this difficulty is at the heart of the single impurity Kondo problem, for which a sound physical picture and quantitative analytical and numerical methods of solution have been developed over a period of 40 years [4]. Over the past 15 years the Kondo problem has attracted renewed interest in the context of electron transport through nanostructures, in particular in situations out of equilibrium. We will discuss impurity models briefly in a later section.

A powerful technique for describing the projection in Hilbert space is the method of auxiliary particles (slave bosons, pseudofermions [5–10]): One assigns an auxiliary field or particle to each of the four states $|0\rangle, |\downarrow\rangle, |\uparrow\rangle, |2\rangle$ at a given lattice site (considering one strongly correlated orbital per site). The Fermi character of the electrons requires that two of the auxiliary particles are fermions, e.g. the ones representing $|\downarrow\rangle, |\uparrow\rangle$ or equally well $|0\rangle, |2\rangle$ and the remaining two are bosons. Introducing new particles for the states $|0\rangle, |2\rangle$ allows to express the projection to the Hilbert space of states without double occupancy as $n_0 + n_\uparrow + n_\downarrow = 1$, where $n_\alpha$ are the occupation numbers of the states $|\alpha\rangle$; i.e. each lattice site is either empty or singly occupied. There are various ways of defining auxiliary particles for a given problem. It is wise to choose the one which is best adapted to the physical properties of the system.

Compared to alternative ways of effecting the projection, the auxiliary particle method has the advantage of allowing one to use the machinery of quantum field theory, i.e. Wick's theorem, diagrammatic perturbation theory and infinite resummations of diagrams, provided the constraint can be incorporated in a satisfactory way.

Historically, auxiliary particle representations have first been introduced in the context of spin models. Spin operators may be represented by Bose operators (Holstein-Primakoff [5], Schwinger [6]) or in the case of spin 1/2 (and with additional complications for higher spins as well) by Fermi operators (Abrikosov [7], Coqblin-Schrieffer [8]). Electron operators necessarily involve a combination of auxiliary fermion and boson operators. The simplest such representation has been proposed for the Anderson impurity problem by Barnes [9], and for lattice problems by Coleman [10]. A more complex representation of electron operators, incorporating the result of the Gutzwiller approximation [11] on the slave boson mean-field level has been developed by Kotliar and Ruckenstein [12]. Generalizations of the latter to manifestly spin rotation invariant form [13] and to particle-hole and spin rotation invariant form [14] have also been proposed. Generalizations to multi-band Hubbard models have been introduced as well [15, 16].

Quite generally, auxiliary particle theories have to deal with two problems: the treatment of the constraint and the approximate description of the dynamics. An accurate control of the constraint alone does not yet make a good theory!

In section 2 we review most of the available pseudoparticle representations for both spin operators and electron operators. Mean-field approximations of slave boson operators within several of the most prominent models are considered in section 3. Section 4 is devoted to Gaussian fluctuation corrections on top of mean-field theories. Chapter 5 is devoted to a class of time-dependent mean-field type approximations, the non-crossing approximation and the conserving T-Matrix approximation. A powerful non-perturbative method allowing to capture collective many-body phenomena is the renormalization group method in its various forms. In section 6 we present several examples of aux-

iliary particle representations employed to describe strong coupling problems within a RG treatment.

## 1.2 Pseudoparticle representations of quantum operators

### 1.2.1 Spin operators

As mentioned in the introduction, the first auxiliary particle represention of quantum operators proposed and successfully applied are the bosonic representations of spin operators by Holstein-Primakoff and by Schwinger. Since both are well documented in the literature we do not consider them here. Generally speaking, bosonic representations are useful to describe ordered states and fluctuations of collective variables. They are less useful if the fermionic character of spin 1/2 particles is of importance. In the following we will concentrate on fermionic representations.

#### Fermionic representations of S=1/2 spins

The spin 1/2 operator $\mathbf{S}$ has a faithful representation in terms of fermion operators $f_\sigma$ ($\sigma = \uparrow, \downarrow$)

$$\mathbf{S} = \frac{1}{2} \sum_{\sigma,\sigma'=\uparrow,\downarrow} f_\sigma^\dagger \boldsymbol{\tau}_{\sigma\sigma'} f_{\sigma'} \tag{1.1}$$

where $\tau$ is the vector of Pauli matrices. The Hilbert space obtained by the creation operators $f_\sigma^\dagger$ acting on the vacuum state $|\mathrm{vac}\rangle$ is spanned by four states. The two unphysical states, the empty and the doubly occupied one, are eliminated by requiring that all states considered are eigenstates of the occupation number operator $Q = \sum_{\sigma=\uparrow,\downarrow} f_\sigma^\dagger f_\sigma$ with eigenvalue $Q = 1$.

#### *Abrikosov projection*

A first projection scheme involves adding a term $\lambda Q$ to the Hamiltonian, and taking the limit $\lambda \to \infty$ [7]. In that case double occupancy is forbidden, while empty states are not involved in expectation values of physical spin operators. The projection of the pseudofermion Green's function $G^<(\omega)$, for example, is effected by taking the following limit $G^<(\omega) = \lim_{\lambda\to\infty}[G^<_\lambda(\omega) Z_\lambda / \langle Q\rangle_\lambda]$. Here $G^<_\lambda(\omega)$ is the pseudofermion Green's function at finite chemical potential $\lambda$, $Z_\lambda$ is the partition function and $\langle Q\rangle_\lambda = \sum_{\sigma=\uparrow,\downarrow} \langle f_\sigma^\dagger f_\sigma\rangle_\lambda$ is the total number of pseudofermions at given $\lambda$. While taking the limit $\lambda \to \infty$ removes the contribution of doubly occupied states, the unphysical contribution of the empty level in the partition function $Z_\lambda$ is removed in the limit $\lambda \to \infty$ by

replacing $Z_\lambda$ by $\langle Q\rangle_\lambda$. In equilibrium, we may now use that $-iG^<_\lambda(\omega) = f(\omega+\lambda)A(\omega) \stackrel{\lambda\to\infty}{\longrightarrow} e^{-\lambda/T}e^{-\omega/T}A(\omega)$, where $f(\omega)$ is the Fermi function, to express the projected Green's function as $G^<(\omega) = ie^{-\omega/T}A(\omega)/[2\int d\omega e^{-\omega/T}A(\omega)]$. Out of equilibrium the occupation function $f_\lambda(\omega)$ has to be calculated from the quantum Boltzmann equation.

The above projection scheme has the disadvantage that particle-hole symmetry is maximally broken. The spectral functions are therefore very unsymmetric under a sign change of $\omega$, causing difficulty in numerical evaluations.

***Particle-hole symmetric projection***

If one takes $\lambda = 0$ the pseudofermion spectral function is particle-hole symmetric, $A(-\omega) = A(\omega)$, which facilitates calculations considerably. In calculating any physical quantity, which only involves spin operators, unphysical states only come in through the partition function, which enters quantities described by diagrams with closed pseudofermion loops. In the case of quantum impurity models, diagrams with more than one pseudofermion loop do not contribute, as each loop introduces a factor $1/N_L$ with $N_L$ the number of lattice sites in the system. The pseudofermion self-energy is not affected, because its relevant diagrams do not contain loops. By contrast, the diagrams for response functions like the conductance and the spin susceptibility necessarily contain one loop. The latter quantities have to be corrected by a normalization factor, as discussed by Larsen [17]. The correction amounts to multiplying the pseudofermion occupation factor $f_\lambda(\omega)$ by a factor

$$Y = Z/Z_p = (Z/Z_0)/[(Z/Z_0) - 1/2]\,, \tag{1.2}$$

where $Z(\lambda) = Tr[e^{-(H+\lambda Q)/T}]$, $Z = Z(\lambda = 0)$ and $Z_0 = Tr[e^{-H_0/T}]$ are the partition functions of the (unprojected) interacting system and noninteracting system (taking $J \to 0$ ), respectively, and $Z_p$ is the physical (projected) partition function. We now calculate $(Z/Z_0)$ by using the relations $Z = Tr[e^{-H/T}] = \frac{1}{2}Z_0 + Z_p$ and $Z\langle Q\rangle = \frac{1}{2}Z_0 + Z_p$. From these two relations we conclude that $\langle Q\rangle = 1$ and that $Y$ is indeed given by the above relation. One may calculate $(Z/Z_0)$ by integrating the total pseudofermion occupation $\langle Q\rangle_\lambda = Z_\lambda^{-1}Tr[Qe^{-(H+\lambda Q)/T}] = -T\frac{d}{d\lambda}\ln Tr[e^{-(H+\lambda Q)/T}]$ with respect to $\lambda$ from 0 to $\infty$. As the spin levels are not occupied in the limit $\lambda \to \infty$ the system is therefore noninteracting in this limit. Hence $\lim_{\lambda\to\infty} Z_\lambda = Z_0/4$ (keeping in mind that the trace over the pseudofermion states at $\lambda = 0$ gives a factor of 4), leading to the result

$$Z/Z_0 = \frac{1}{4}\exp[\frac{1}{T}\int_0^\infty d\lambda\,\langle Q\rangle_\lambda]\,. \tag{1.3}$$

In this set-up the total occupation number may be calculated approximately from $\int_0^\infty d\lambda\,\langle Q\rangle_\lambda = \frac{1}{T}\int_0^\infty d\lambda 2\int d\omega f(\omega+\lambda)A(\omega) \approx 2\int d\omega \ln(1+e^{-\omega/T})A(\omega)$,

neglecting the $\lambda$-dependence of the spectral function $A(\omega)$. In the case of the spin 1/2 Kondo model the factor $Y$ increases from $Y = 1$ at low temperatures ($T \ll T_K$, the Kondo temperature) to $Y = 2$ at $T \gg T_K$.

***Popov-Fedotov projection***

A different approach allowing for an exact treatment of the constraint even for lattice systems has been proposed by Popov and Fedotov [18]. It amounts to applying a homogeneous, *imaginary-valued* chemical potential $\mu^{\rm ppv} = -\frac{i\pi T}{2}$, where $T$ is the temperature. Thus, within this scheme, the Hamiltonian $H$ is replaced by

$$H \longrightarrow H^{\rm ppv} = H - \mu^{\rm ppv} \sum_i Q_i \quad . \tag{1.4}$$

Note that $H$ denotes a given spin-1/2 Hamiltonian using the fermionic representation of spin operators. Given a physical operator $\mathcal{O}$ (i.e., an arbitrary sum or product of spin operators) it can be shown [19] that the expectation value $\langle\mathcal{O}\rangle^{\rm ppv}$, calculated with $H^{\rm ppv}$ and the *entire* Hilbert space, is identical to the physical expectation value $\langle\mathcal{O}\rangle$, where the average is performed with the original Hamiltonian $H$. The projection works by virtue of a mutual cancellation of the unphysical contributions of the sectors $Q_i = 0$ and $Q_i = 2$, at each site. It should be emphasized that, although the Hamiltonian $H^{\rm ppv}$ is no longer hermitian, the quantity $\langle\mathcal{O}\rangle^{\rm ppv}$ comes out real-valued. If, on the other hand, $\mathcal{O}$ is unphysical in the sense that it is non-zero in the unphysical sector, e.g., the operator $\mathcal{O} = Q_i$, the expectation value $\langle Q_i\rangle^{\rm ppv}$ is meaningless and one has $\langle Q_i\rangle \neq \langle Q_i\rangle^{\rm ppv}$.

This approach is applicable to spin models [19–22] but unfortunately it can not be extended to cases away from half filling. Although $\mu^{\rm ppv}$ vanishes in the limit $T \to 0$, in principle the exact projection with $\mu = \mu^{\rm ppv}$ and the average projection with $\mu = 0$ are not equivalent at $T = 0$. This is due to the fact that the computation of an average $\langle \dots \rangle^{\rm ppv}$ does not necessarily commute with the limit $T \to 0$. Nevertheless it can be expected that in usual quantum spin models both projection schemes are equivalent at $T = 0$. This can be understood with the following argument: Starting from the physical ("true") ground state, a fluctuation of one fermion charge results in two sites with unphysical occupation numbers, one with no and one with two fermions. Since these sites carry spin zero the sector of the Hamiltonian with that occupation is identical to the physical Hamiltonian where the two sites are effectively *missing*. Thus a fluctuation from the ground state into this sector costs the binding energy of the two sites which is of the order of the exchange coupling, even in the case of strong frustration. Consequently, at $T = 0$ charge fluctuations are not allowed and it is sufficient to use the simpler average projection with $\mu = 0$.

### 1.2.2 Electron operators

The Hilbert space of electrons in a local orbital is spanned by four states: Two with single occupancy (representing a local spin 1/2) and the empty and doubly occupied states. Obviously, the singly occupied states have fermionic character, while the remaining two states have bosonic character. One may now envisage to create these states out of a vacuum state $|\mathrm{vac}\rangle$, which is defined by the absence of any of the four occupation number states. These four states may then be created by fermionic or bosonic auxiliary operators. This may be done in a multitude of ways. We will concentrate here on the representations introduced by Barnes [9] and by Kotliar and Ruckenstein [12].

#### Barnes's representation

The basic idea consists in locally decomposing the electronic excitations into spin and charge components. This can be achieved in many different ways. A suitable Hubbard-Stratonovich decoupling of the interaction term could reach this goal, but would likely be limited to weak interaction. Instead, in the pioneering Barnes approach [9] the spin and charge degrees of freedom are represented by fermionic and bosonic operators, respectively. Being more numerous than the original (physical) operators, the auxiliary operators span a Fock space that is larger than the physical one. Consequently they need to fulfill an appropriate set of constraints for such a representation to be faithful. Specifically Barnes considered the single impurity Anderson model (SIAM):

$$H = \sum_{\boldsymbol{k}\sigma} \varepsilon_{\boldsymbol{k}} c^\dagger_{\boldsymbol{k}\sigma} c_{\boldsymbol{k}\sigma} + \varepsilon_f \sum_\sigma a^\dagger_\sigma a_\sigma + V \sum_{\boldsymbol{k}\sigma} \left( c^\dagger_{\boldsymbol{k}\sigma} a_\sigma + a^\dagger_\sigma c_{\boldsymbol{k}\sigma} \right) + U a^\dagger_\uparrow a_\uparrow a^\dagger_\downarrow a_\downarrow \,. \tag{1.5}$$

Clearly, this problem may not be treated by means of perturbation theory in $U$, especially in the $U \to \infty$ limit. Instead, Barnes introduced the auxiliary fermionic ($f_\sigma$) and bosonic ($e, d$) operators in terms of which the physical electron operators $a_\sigma$ read,

$$a_\sigma = e^\dagger f_\sigma + \sigma f^\dagger_{-\sigma} d \tag{1.6}$$

The $a_\sigma$-operators obey the ordinary Fermion anticommutation relations. This property is not automatically preserved when using the representation Eq. 1.6, even when the fermionic and bosonic auxiliary operators obey canonical commutation relations. In addition the constraint

$$Q \equiv e^\dagger e + \sum_\sigma f^\dagger_\sigma f_\sigma + d^\dagger d = 1 \tag{1.7}$$

must be satisfied. Eq. 1.6 together with Eq. 1.7 constitutes a faithful representation of the physical electron operator in the sense that both have the

same matrix elements in the physical Hilbert subspace with $Q = 1$. The above representation has been widely used, in particular in the $U \to \infty$ limit where the operator $d$ (linked to double occupancy) drops out. The constraint can be implemented by means of a functional integral representation. For example, for $U \to \infty$ the partition function, projected onto the $Q = 1$ subspace, reads,

$$Z = \int_{-\pi/\beta}^{\pi/\beta} \frac{\beta d\lambda}{2\pi} e^{i\beta\lambda} \int \prod_{\sigma} D[f_\sigma, f_\sigma^\dagger] \int \prod_{\boldsymbol{k}\sigma} D[c_{\boldsymbol{k}\sigma}, c_{\boldsymbol{k}\sigma}^\dagger] \int D[e, e^\dagger] \mathrm{e}^{-\int_0^\beta d\tau (\mathcal{L}_f(\tau) + \mathcal{L}_b(\tau))} \tag{1.8}$$

with the fermionic and bosonic Lagrangians

$$\begin{aligned} \mathcal{L}_f(\tau) &= \sum_{\boldsymbol{k}\sigma} c_{\boldsymbol{k}\sigma}^\dagger(\tau)(\partial_\tau + \varepsilon_{\boldsymbol{k}} - \mu) c_{\boldsymbol{k}\sigma}(\tau) + \sum_\sigma f_\sigma^\dagger(\tau)(\partial_\tau + \varepsilon_c - \mu + i\lambda) f_\sigma(\tau) \\ &\quad + V \sum_{\boldsymbol{k}\sigma} \left( c_{\boldsymbol{k}\sigma}^\dagger(\tau) f_\sigma(\tau) e^\dagger(\tau) + h.\ c. \right) \\ \mathcal{L}_b(\tau) &= e^\dagger(\tau)(\partial_\tau + i\lambda) e(\tau)\,. \end{aligned} \tag{1.9}$$

Here the $\lambda$ integration enforces the constraint, and the Lagrangian is bi-linear in the fermionic fields. Remarkably, this has been achieved without decoupling the interaction term. Besides, the correctness of the representation can be verified by carrying out all integrals in, e.g., the $V \to 0$ limit. By virtue of the substitution $z = e^{-i\beta\lambda}$, $\beta d\lambda = idz/z$, the $\lambda$ integral in Eq. 1.8 is transformed into a contour integral along the complex unit circle. Observing that this substitution implies exactly a 2nd-order pole at $z = 0$ (i.e., at $i\lambda \to +\infty$, real), it is seen that the projection of $Z$ amounts to calculating the grand canonical Q expectation value in the limit of infinite, real chemical potential, $Z = \lim_{i\lambda\to\infty} \langle Q \rangle_{i\lambda}$ [23], equivalent to the Abrikosov projection. Eq. 1.8 may also be viewed as the projection of the non-interacting partition function onto the "$U = \infty$"-subspace. Indeed Eq. 1.8 may be rewritten as:

$$Z = P \prod_\sigma \det\left[S_\sigma[e(\tau), \lambda]\right] \tag{1.10}$$

with $\det\left[S_\sigma[e(\tau), \lambda]\right]$ the fermionic determinant for one spin species involving an effective time-dependent hybridization ($Ve^\dagger(\tau)$), and the projection operator:

$$P = \int_{-\pi/\beta}^{\pi/\beta} \frac{\beta d\lambda}{2\pi} \mathrm{e}^{i\beta\lambda} \int D[e, e^\dagger] e^{-\int_0^\beta d\tau \mathcal{L}_b(\tau)}\,, \tag{1.11}$$

Yet, there is an asymmetry in the representation of spin and charge degrees of freedom. While the latter can be expressed in terms of bosons, this is not the case of the former, and may cause unnecessary errors in any approximate treatment (for details see Ref. [14]).

With this motivation Kotliar and Ruckenstein introduced a representation where spin and charge degrees of freedom may be expressed by bosons.

**Kotliar and Ruckenstein representation**

In the Kotliar and Ruckenstein (KR) representation two additional Bose operators linked to the spin degrees of freedom (DoF) are introduced, $p_\downarrow$ and $p_\uparrow$ [12]. In this approach the physical electron operators are represented as:

$$a_\sigma = \tilde{z}_\sigma f_\sigma \quad \text{with} \quad \tilde{z}_\sigma = e^\dagger p_\sigma + p^\dagger_{-\sigma} d \tag{1.12}$$

where the first term corresponds to the transition from the singly occupied state to the empty one, and the second term to the transition from the doubly occupied state to the singly occupied one. Again the representation is faithful provided the auxiliary operators obey canonical commutation relations and satisfy constraints. They read,

$$e^\dagger e + \sum_\sigma p^\dagger_\sigma p_\sigma + d^\dagger d = 1 \tag{1.13}$$

$$p^\dagger_\sigma p_\sigma + d^\dagger d = f^\dagger_\sigma f_\sigma \qquad \sigma = \uparrow, \downarrow \ . \tag{1.14}$$

They may be enforced in a functional integral representation with Lagrange multipliers in a fashion analogous to the one we encoutered with the Barnes representation. Besides, the density operator ($\sum_\sigma p^\dagger_\sigma p_\sigma + 2 d^\dagger d$) and the z-component of the spin operator ($\frac{1}{2}\sum_{\sigma=\stackrel{+}{-}} \sigma p^\dagger_\sigma p_\sigma$) may be expressed in terms of bosons. Spin and charge DoF may therefore be treated on equal footing. This procedure can be extended to multiband models [15].

**Spin-rotation invariant representation**

Though faithful, the Kotliar and Ruckenstein representation is lacking spin rotational invariance as transverse components of the spin operator may not be simply represented in terms of auxiliary operators. Indeed, $S^{x,y}$ is neither related to $\frac{1}{2}\sum_{\sigma\sigma'} f^\dagger_\sigma \tau^{x(y)}_{\sigma\sigma'} f_{\sigma'}$ nor to $\frac{1}{2}\sum_{\sigma\sigma'} p^\dagger_\sigma \tau^{x(y)}_{\sigma\sigma'} p_{\sigma'}$. Hence fluctuations associated to the transverse modes are not treated on the same footing as the ones associated to the longitudinal mode. With this motivation a manifestly spin-rotation invariant (SRI) formulation has been introduced [13,14]. In this setup the doublet $p_\sigma$ [12] is replaced by a scalar (S=0) field $p_0$ and a vector (S=1) field $\boldsymbol{p} = (p_x, p_y, p_z)$, in terms of which the state $|\sigma\rangle = a^\dagger_\sigma |0\rangle$ may be represented as

$$|\sigma\rangle = \sum_{\sigma'} p^\dagger_{\sigma\sigma'} f^\dagger_{\sigma'} |\text{vac}\rangle \quad \text{with} \quad p^\dagger_{\sigma\sigma'} = \frac{1}{2} \sum_{\mu=0,x,y,z} p^\dagger_\mu \tau^\mu_{\sigma\sigma'} \, . \tag{1.15}$$

The bosons $p_\mu$ obey canonical commutation relations, and all the auxiliary operators annihilate the vacuum ($f_\sigma|\mathrm{vac}\rangle = e|\mathrm{vac}\rangle = \ldots|\mathrm{vac}\rangle = 0$). With this at hand the electron operators may be written as:

$$a_\sigma = \sum_{\sigma'} f_{\sigma'} \tilde{z}_{\sigma'\sigma} \quad \text{with} \quad \tilde{z}_{\sigma'\sigma} = e^\dagger p_{\sigma'\sigma} + \sigma'\sigma p^\dagger_{-\sigma,-\sigma'} d\,. \tag{1.16}$$

Again, the auxiliary operators need to satisfy constraints. They read,

$$e^\dagger e + \sum_\mu p^\dagger_\mu p_\mu + d^\dagger d = 1 \tag{1.17}$$

$$\sum_\sigma f^\dagger_\sigma f_\sigma = \sum_\mu p^\dagger_\mu p_\mu + d^\dagger d \tag{1.18}$$

$$\sum_{\sigma,\sigma'} f^\dagger_{\sigma'} \boldsymbol{\tau}_{\sigma\sigma'} f_\sigma = p^\dagger_0 \boldsymbol{p} + \boldsymbol{p}^\dagger p_0 - i\boldsymbol{p}^\dagger \times \boldsymbol{p} \ . \tag{1.19}$$

While the density operator ($n = \sum_\mu p^\dagger_\mu p_\mu + 2d^\dagger d$), and the density of doubly occupied sites operator ($D = d^\dagger d$) may be expressed in terms of bosons or fermions, the spin operator reads,

$$\boldsymbol{S} = \sum_{\sigma\sigma'\sigma_1} \boldsymbol{\tau}_{\sigma\sigma'} p^\dagger_{\sigma\sigma_1} p_{\sigma_1\sigma'}\,. \tag{1.20}$$

This expression is especially useful in the context of the t-J model, in particular because the spin degrees of freedom need not be expressed in terms of the original fermions. Using the above, one can tackle models of correlated electrons such as the single impurity Anderson model, the Anderson lattice model, the t-J or the Hubbard model. However, while the spin and charge degrees of freedom have been mapped onto bosons, anomalous propagators necessarily vanish on a saddle-point level as the Lagrangian is bi-linear in the fermionic fields, independent of the model. Here they are not treated on equal footing with the spin and charge degrees of freedom. This motivated two of us to introduce a manifestly spin- and charge-rotation-invariant formulation (SCRI) [14].

### Spin- and charge-rotation-invariant formulation

The SCRI representation is motivated both by the need to be able to account for anomalous expectation values (such as the ones arising when investigating excitonic states), and to satisfy the particle-hole rotational symmetry entailed in many models. The generators of these rotations are given by the components of the operators:

$$\boldsymbol{J} = \frac{1}{2}\left(a^\dagger_\uparrow, a_\downarrow\right) \boldsymbol{\tau} \begin{pmatrix} a_\uparrow \\ a^\dagger_\downarrow \end{pmatrix} \tag{1.21}$$

which form a spin algebra with the usual commutation relations. One may then replace the doublet $e$, $d$ by a scalar (vector) $b_0$ ($\boldsymbol{b}$) field (with respect to rotations in the particle-hole space), all of them satisfying canonical commutation relations. In terms of them the two local occupation number states $|2\rangle \equiv |+\rangle$, and $|0\rangle \equiv |-\rangle$ may be represented as:

$$|\rho\rangle = \sum_{\rho'} b^\dagger_{\rho\rho'} \psi^\dagger_{\rho'} |\mathrm{vac}\rangle \quad ; \quad \rho = \pm \tag{1.22}$$

with $\psi^\dagger_+ = f^\dagger_\uparrow f^\dagger_\downarrow$ and $\psi^\dagger_- = 1$. When considering the generalized $\tilde{z}$-operator $\tilde{z}_{\rho\sigma,\rho'\sigma'} = \rho\rho' b^\dagger_{-\rho,-\rho'} p_{\sigma'\sigma} + \sigma\sigma' p^\dagger_{-\sigma,-\sigma'} b_{\rho'\rho}$ (with $b^\dagger_{\rho\rho'} = \frac{1}{2}\sum_{\mu=0,x,y,z} b^\dagger_\mu \tau^\mu_{\rho\rho'}$) and the matrix operators:

$$A_{\rho,\sigma} = \begin{pmatrix} a_\uparrow & a_\downarrow \\ a^\dagger_\downarrow & -a^\dagger_\uparrow \end{pmatrix} \quad \text{and} \quad F_{\rho,\sigma} = \begin{pmatrix} f_\uparrow & f_\downarrow \\ f^\dagger_\downarrow & -f^\dagger_\uparrow \end{pmatrix} \tag{1.23}$$

one may write the physical electron operator as:

$$A_{\rho\sigma} = \sum_{\sigma',\rho'} \tilde{z}_{\rho\sigma,\rho'\sigma'} F_{\rho'\sigma'} \,. \tag{1.24}$$

The constraints now read,

$$\begin{aligned} f^\dagger_{\sigma'} f_\sigma &= 2\sum_{\sigma_1} p^\dagger_{\sigma_1\sigma} p_{\sigma'\sigma_1} + \frac{1}{2}\delta_{\sigma,\sigma'} \sum_{\mu=0,x,y,z} b^\dagger_\mu b_\mu \\ \sum_\sigma F^\dagger_{\rho\sigma} F_{\rho'\sigma} &= 2\sum_{\rho_1} b^\dagger_{\rho_1\rho} b_{\rho'\rho_1} + \frac{1}{2}\delta_{\rho,\rho'} \sum_{\mu=0,x,y,z} p^\dagger_\mu p_\mu \,. \end{aligned} \tag{1.25}$$

In particular, when performing the trace of Eq. 1.25, one obtains:

$$\sum_\sigma f^\dagger_\sigma f_\sigma = 1 \quad ; \quad \sum_{\mu=0,x,y,z} \left( p^\dagger_\mu p_\mu + b^\dagger_\mu b_\mu \right) = 1 \,. \tag{1.26}$$

Therefore, both spin and charge DoF no longer possess a representation in terms of the auxiliary fermions. Instead, correcting Eq. (48) in [14], the density operator reads,

$$n = \sum_\mu p^\dagger_\mu p_\mu + 2D \tag{1.27}$$

with the density of doubly occupied sites:

$$D = \frac{1}{2}\sum_{\mu\mu'} b^\dagger_\mu b_{\mu'} \mathrm{tr}\left[ \left(\tau^0 + \tau^z\right) \tau^\mu \tau^{\mu'} \right] \,. \tag{1.28}$$

The spin operator is still given by Eq. 1.20. The SCRI representation of the Hubbard model is thus obtained using Eq. 1.24 and Eq. 1.28, together with the constraints Eq. 1.25.

**Gauge symmetry and radial slave boson fields**

When representing the electron operators $a_\sigma$ as $\tilde{z}_\sigma f_\sigma$, it is immediately clear that the latter expression is invariant under the group of transformations:

$$f_\sigma(\tau) \longrightarrow f_\sigma(\tau) e^{i\phi(\tau)}\,, \quad \text{and} \quad \tilde{z}_\sigma(\tau) \longrightarrow \tilde{z}_\sigma(\tau) e^{-i\phi(\tau)}\,. \tag{1.29}$$

This local $U(1)$ gauge symmetry was first realized by Read and Newns [24] in the context of the $U \to \infty$ Barnes representation for the SIAM (with $\tilde{z}_\sigma = e^\dagger$). In that case this can be made use of to gauge away the phase of the slave boson, which remains as a purely radial field, while the constraint Lagrange parameter is promoted to a time-dependent field. Yet, standard textbooks do not mention representations of such radial fields that are set up on a discretized time mesh from the beginning.

A scheme specific to radial slave boson fields has been proposed by one of us [25]. In this scheme the partition function takes a form analogous to Eq. 1.8. However the projection operator does not mix the $N$ time steps, and may be written as:

$$\begin{aligned} P &= \lim_{N\to\infty} \lim_{W\to\infty} \prod_{n=1}^{N} P_n\,, \quad \text{with} \\ P_n &= \int_{-\infty}^{\infty} \frac{\beta}{N} \frac{d\lambda_n}{2\pi} \int_{-\infty}^{\infty} dx_n \mathrm{e}^{-\frac{\beta}{N}(i\lambda_n(x_n-1)+Wx_n(x_n-1))}\,. \end{aligned} \tag{1.30}$$

Here the constraint parameter $\lambda_n$ is defined for each time step $n$, i.e., it is a time-dependent field, and x represents the radial slave boson field. In the discrete time step form, the fermionic part of the action reads,

$$\begin{aligned} S_f = \sum_{n=1}^{N} \Bigg\{ & \sum_{\boldsymbol{k}\sigma} c^\dagger_{\boldsymbol{k},n,\sigma} \left( c_{\boldsymbol{k},n,\sigma} - e^{-\frac{\beta}{N}(\varepsilon_{\boldsymbol{k}}-\mu)} c_{\boldsymbol{k},n-1,\sigma} \right) \\ & + \sum_{\sigma} f^\dagger_{n,\sigma} \left( f_{n,\sigma} - e^{-\frac{\beta}{N}(\varepsilon_f + i\lambda_n - \mu)} f_{n-1,\sigma} \right) \\ & + \frac{\beta}{N} \sum_{\boldsymbol{k}\sigma} V x_n \left( c^\dagger_{\boldsymbol{k},n,\sigma} f_{n-1,\sigma} + f^\dagger_{n,\sigma} c_{\boldsymbol{k},n-1,\sigma} \right) \Bigg\}\,. \end{aligned} \tag{1.31}$$

The integration over the fermionic fields can be carried out, and the partition function can be obtained by projecting the resulting fermionic determinant:

$$Z = P \prod_{\sigma} \det\left[ S_\sigma\left[\{x_n\}, \{\lambda_n\}\right]\right] \tag{1.32}$$

with the above projection operator Eq. 1.30. The expectation value of the hole density operator takes the simple form:

$$\langle n_h(\tau_m)\rangle = \langle x_m \rangle = \frac{1}{Z} P \left\{ x_m \prod_{\sigma} \det\left[ S_\sigma\left[\{x_n\}, \{\lambda_n\}\right]\right] \right\}\,. \tag{1.33}$$

It is easily seen to be time-independent. In contrast to a Bose condensate $\langle x_m \rangle$ is generically finite, and may only vanish for zero hole concentration [26]. Another specific feature of the radial slave boson field is that, for any power $a > 0$, one finds $\langle x_m^a \rangle = \langle x_m \rangle$, as the corresponding projections of the fermionic determinant all yield the same value.

The hole autocorrelation function may also be expressed as a projection of the fermionic determinant. It reads,

$$\langle n_h(\tau_n) n_h(\tau_m) \rangle = \langle x_n x_m \rangle = \frac{1}{Z} P \left\{ x_n x_m \prod_\sigma \det \left[ S_\sigma \left[ \{x_n\}, \{\lambda_n\} \right] \right] \right\} . \tag{1.34}$$

Regarding the Kotliar and Ruckenstein representation the determination of the gauge symmetry group has been debated over several years [14, 27–30]. It was finally agreed that it reads $U(1) \times U(1) \times U(1)$. By promoting all three constraint parameters to fields one may gauge away the phase of three bosonic fields, the fourth one, for example $d$, remaining complex. Therefore, in the $U \to \infty$ limit ($d \to 0$), the three remaining bosonic fields are radial slave boson fields. In functional integral language they may be handled in the same fashion as the above x-field.

## 1.3 Mean-field approximations

An economical and often physically reasonable way to determine observable quantities in the SB framework is provided by a saddle-point approximation (SPA) to the functional integral. This is equivalent to allowing for a finite expectation value of a Bose field amplitude. Strictly speaking, a finite expectation value of a Bose field operator violates gauge invariance and should not exist. In contrast, a finite saddle-point amplitude of the radial slave boson fields is compatible with Elitzur's theorem.

### 1.3.1 Saddle-point approximation to the Barnes representation

In its simplest form the SPA consists of replacing the boson field operators $b_i$ at each lattice site, or $b$ at the impurity site, by the modulus of its expectation value, in accordance with the above. The remaining problem is a non-interacting model, which is easily solved. We will discuss the solution briefly for the Anderson impurity model and the Anderson lattice model.

#### Kondo effect in the Anderson impurity model

In SPA the Anderson impurity Hamiltonian Eq. 1.5 takes the form

$$H = \sum_{\boldsymbol{k}\sigma} \varepsilon_{\boldsymbol{k}} c^\dagger_{\boldsymbol{k}\sigma} c_{\boldsymbol{k}\sigma} + \varepsilon_f \sum_\sigma f^\dagger_\sigma f_\sigma + V \sum_{\boldsymbol{k}\sigma} e_0 \left( c^\dagger_{\boldsymbol{k}\sigma} f_\sigma + f^\dagger_\sigma c_{\boldsymbol{k}\sigma} \right) + \lambda(Q-1) \tag{1.35}$$

where the conserved charge is $Q = \sum_\sigma f^\dagger_\sigma f_\sigma + e_0^2 = 1$ and $\lambda$ is the corresponding Lagrange multiplier. This is nothing but a resonant level model with renormalized parameters. $\widetilde{\varepsilon}_f = \varepsilon_f + \lambda$ and $\widetilde{V} = V e_0$. At the stationary point of the free energy one finds that the level position $\widetilde{\varepsilon}_f$ and the level width $\widetilde{\Delta} = e_0^2 \Delta = \pi N_0 \widetilde{V}^{\,2}$, where $\Delta = \pi N_0 V^2$ ($N_0 = 1/2D$ is the conduction electron DOS at the Fermi level), satisfy the equations

$$\widetilde{\varepsilon}_f = \varepsilon_f - \frac{2\Delta}{\pi} \ln \frac{\sqrt{\widetilde{\varepsilon}_f^2 + \widetilde{\Delta}^2}}{D} \tag{1.36}$$

$$\widetilde{\Delta} = \Delta - \frac{2\Delta}{\pi} \tan^{-1} \frac{\widetilde{\Delta}}{\widetilde{\varepsilon}_f} \tag{1.37}$$

In the limit of $\Delta \ll |\varepsilon_f|$ the occupation of the local level, $n_f = \frac{2}{\pi} \tan^{-1} \frac{\widetilde{\Delta}}{\widetilde{\varepsilon}_f}$, approaches unity, which means that a local moment forms at higher temperature. Below a characteristic temperature, the Kondo temperature $T_K$, the local moment gets screened by the conduction electron spins, which form a resonance state with the local moment, located close to the Fermi energy, at $\widetilde{\varepsilon}_f$, and of width $\widetilde{\Delta} \approx T_K = D \exp \frac{-|\varepsilon_f|}{2N_0 V^2} = D \exp \frac{1}{2N_0 J}$, where $J = \frac{V^2}{|\varepsilon_f|}$ is the antiferromagnetic spin exchange coupling constant of the local spin and the local conduction electron spin density. The low temperature behavior of Kondo systems is reasonably well described by slave boson mean-field theory. At higher temperatures one finds in this approximation a spurious first order transition to the local moment regime, rather than a continuous crossover.

### Heavy fermions in the Anderson lattice model

The SB mean-field approximation to the Anderson lattice model in the limit $U \to \infty$ [24] leads to the following single-particle Hamiltonian of two hybridized bands

$$H = \sum_{\boldsymbol{k}\sigma} \varepsilon_{\boldsymbol{k}} c^\dagger_{\boldsymbol{k}\sigma} c_{\boldsymbol{k}\sigma} + \varepsilon_f \sum_{i,\sigma} f^\dagger_{i\sigma} f_{i\sigma} + V \sum_{i,\sigma} e_0 \left( c^\dagger_{i\sigma} f_{i\sigma} + f^\dagger_{i\sigma} c_{i\sigma} \right) + \sum_i \lambda_i (Q_i - 1) \tag{1.38}$$

The stationarity condition with respect to the fields $\lambda_i$ leads to the condition $\langle Q_i \rangle = 1$,which for a translation invariant state is independent of the lattice position $\mathbf{R}_i$. As in the impurity problem the $f-$level position is shifted by the correlation effect to $\widetilde{\varepsilon}_f = \varepsilon_f + \lambda = \varepsilon_f - 2N_0 V^2 \ln \frac{\widetilde{\varepsilon}}{D}$ and the square of the boson amplitude is related to the $f-$level occupation $n_f$

$$\widetilde{\varepsilon}_f = \varepsilon_f - 2N_0V^2 \ln \frac{\widetilde{\varepsilon}_f - \varepsilon_F}{D} \tag{1.39}$$

$$e_0^2 = 1 - n_f = 1 - \frac{2N_0V^2e_0^2}{\widetilde{\varepsilon}_f} \tag{1.40}$$

Here we have assumed $|\widetilde{\varepsilon}_f| \ll D$. We observe that, provided $\varepsilon_f$ is sufficiently below the Fermi level $\varepsilon_F$, we have $|\widetilde{\varepsilon}_f| \ll |\varepsilon_f|$ and it follows from Eq. 1.39 that $\widetilde{\varepsilon}_f - \varepsilon_F = D \exp \frac{-|\varepsilon_f|}{2N_0V^2} = T_K$, equal to the single impurity Kondo temperature. In this limit $e_0^2 \approx |\widetilde{\varepsilon}_f|/2N_0V^2 \ll 1$ and the hybridization amplitude is substantially reduced, leading to heavy quasiparticle bands of energy

$$E_{\boldsymbol{k}}^{\pm} = \frac{1}{2}[\varepsilon_{\boldsymbol{k}} + \widetilde{\varepsilon}_f \pm \sqrt{(\varepsilon_{\boldsymbol{k}} + \widetilde{\varepsilon}_f)^2 + V^2e_0^2}] \tag{1.41}$$

### 1.3.2 Saddle point approximation to the KR representation

It is tempting to extend this approach to the Hubbard Model. Yet, at this stage of the formulation, the representation suffers from the following drawback: The non-interacting limit is not properly recovered on the SPA level (see [12] for the case of the Hubbard model), in contrast to more conventional approaches. This can be cured by noticing that there is no unique slave boson representation, but rather infinitely many different ones. They are all equivalent when the functional integral is exactly evaluated, but differ on saddle-point level. Fortunately enough, there is one representation of the kinetic energy which allows to overcome the above drawback. For the KR representation it consists in replacing the operators $\tilde{z}_\sigma$ in Eq. 1.12 by

$$z_\sigma = e^\dagger L_\sigma R_\sigma p_\sigma + p_{-\sigma}^\dagger L_\sigma R_\sigma d \quad \text{with} \tag{1.42}$$

$$L_\sigma = \frac{1}{\sqrt{1 - p_\sigma^\dagger p_\sigma - d^\dagger d}} \quad \text{and} \quad R_\sigma = \frac{1}{\sqrt{1 - p_{-\sigma}^\dagger p_{-\sigma} - e^\dagger e}}\,, \tag{1.43}$$

and to consistently use $a_\sigma = z_\sigma f_\sigma$ in the representation of the kinetic energy operator. In this form the SPA to the KR representation is equivalent to the Gutzwiller approximation to the Gutzwiller wave-function [12]. As the latter two are equivalent in the large $d$ limit, the SPA to the KR representation turns variationally controlled in this limit. In adddition it turns exact in several large $N$ limits [14], or for particular toy models [31]. These properties are shared by the SRI formulation [14]. Indeed, introducing $\tilde{p}_{\sigma\sigma'} \equiv \sigma\sigma' p_{-\sigma',-\sigma}$ the z-operator reads,

$$\underline{z} = e^\dagger \underline{L}\ M\ \underline{R}\ \underline{p}\ + \underline{\tilde{p}}^\dagger \underline{L}\ M\ \underline{R}\ d \tag{1.44}$$

with

$$M = \left[1 + e^\dagger e + \sum_\mu p_\mu^\dagger p_\mu + d^\dagger d\right]^{\frac{1}{2}} \quad \text{and} \tag{1.45}$$

$$\underline{L} \;= \left[\left(1 - d^\dagger d\right)\underline{1} - 2\underline{p}^\dagger \underline{p}\;\right]^{-\frac{1}{2}} \quad \text{and} \quad \underline{R} = \left[\left(1 - e^\dagger e\right)\underline{1} - 2\underline{\tilde{p}}^\dagger \underline{\tilde{p}}\;\right]^{-\frac{1}{2}} . \tag{1.46}$$

Eq. 1.44 and Eq. 1.46 corrects Eq. (22) in [14] and Eq. 1.46 corrects Eq. (3) in [32].

### Mott-Hubbard metal-insulator transition

The KR and SRI representations have been used to characterize a very broad range of phases of the Hubbard Model [33–45]. In addition to the above discussed motivations, the popularity of the approach is fueled by its ability to describe a Mott metal-to-insulator transition as it encompasses the Brinkman-Rice mechanism [46,47] that we describe below. It arises when considering the paramagnetic saddle-point. In the SRI representation it corresponds to set the bosonic fields $\boldsymbol{p}_i(\tau)$ and the constraint fields enforcing Eq. 1.19 to zero, and to replace the remaining bosonic and constraint fields by their mean value. The free energy then reads,

$$F = -T\sum_{\boldsymbol{k},\sigma} \ln\left(1 + \mathrm{e}^{-\frac{E_{\boldsymbol{k}\sigma}}{T}}\right) + Ud^2 + \alpha\left(e^2 + p_0^2 + d^2 - 1\right) - \beta_0\left(p_0^2 + 2d^2\right) \tag{1.47}$$

Here the Lagrange multiplier $\alpha$ ($\beta_0$) enforces the constraint Eq. 1.17 (Eq. 1.18). The quasiparticle dispersion relation is given by:

$$E_{\boldsymbol{k}\sigma} = z_0^2 t_{\boldsymbol{k}} + \beta_0 - \mu \tag{1.48}$$

with

$$z_0 = \frac{1}{\sqrt{2}} \frac{p_0(e+d)}{\sqrt{1 - d^2 - \frac{1}{2}p_0^2}\sqrt{1 - e^2 - \frac{1}{2}p_0^2}} . \tag{1.49}$$

$z_0^2$ both plays the role of a mass renormalization factor and of a quasiparticle residue. Should it vanish in some parameter range, then a Mott insulating state would be realized. Solving the saddle-point equations at half-filling yields:

$$z_0^2 = 1 - \left(\frac{U}{U_0}\right)^2 \tag{1.50}$$

with

$$U_0 = -4 \sum_{\boldsymbol{k},\sigma} t_{\boldsymbol{k}} f_F(E_{\boldsymbol{k},\sigma}) \tag{1.51}$$

Therefore, the quasiparticle residue continuously varies from 1 down to 0 for $U \to U_0$. There, the quasiparticle mass diverges, its residue vanishes, and a Mott gap opens. Indeed, solving the equation for the chemical potential of the quasiparticles for $U > U_0$ and $n \to 1$ yields:

$$\mu(n) = \frac{U}{2}\left[1 - \frac{1-n}{|1-n|}\sqrt{1-\frac{U_0}{U}}\right] \tag{1.52}$$

The discontinuity in $\mu$ across n=1 indicates a pair of first order phase transitions from the metallic phase at $n < 1$ (with finite $z_0$) to the insulating phase at $n = 1$ (with chemical potential $\mu = \frac{U}{2}$) and back to the metallic phase at $n > 1$ (with finite $z_0$). This discontinuity vanishes for $U \to U_0^+$, which is therefore a critical point. In the insulating phase the quasiparticle contribution to doubly occupied sites vanishes. This does not imply that the latter is predicted to be zero, but that it purely results from fluctuations, that we address in Sec. 1.4.

### Magnetic order in the Anderson lattice model

The Anderson lattice model is believed to describe the physics of many transition-metal, rare-earth and actinide compounds, including the so-called heavy fermion compounds. It is one of the archetypical models of correlated electrons on a lattice, consisting of a "light" conduction band hybridized with a strongly correlated narrow f-electron band. Depending on the strength of the onsite Coulomb repulsion on the f-orbital, the hybridization strength, the band filling, the model describes either localized moments interacting via spin exchange interaction (e.g. the RKKY interaction), which usually order at low temperature, or Kondo screened moments and heavy quasiparticles. The competition between these two ground states gives rise to a quantum phase transition [48, 49]. A qualitatively correct description (excluding the critical behavior at the quantum critical point, which requires a different approach) may be obtained within the SRI slave boson mean-field theory. The Hamiltonian of the Anderson lattice model reads,

$$\begin{aligned} H = &\sum_{\boldsymbol{k}\sigma} \varepsilon_{\boldsymbol{k}} c^\dagger_{\boldsymbol{k}\sigma} c_{\boldsymbol{k}\sigma} + \varepsilon_a \sum_{i,\sigma} a^\dagger_{i\sigma} a_{i\sigma} + V \sum_{i,\sigma} \left( c^\dagger_{i\sigma} a_{i\sigma} + a^\dagger_{i\sigma} c_{i\sigma} \right) \\ &+ U \sum_i a^\dagger_{i\uparrow} a_{i\uparrow} a^\dagger_{i\downarrow} a_{i\downarrow} \end{aligned} \tag{1.53}$$

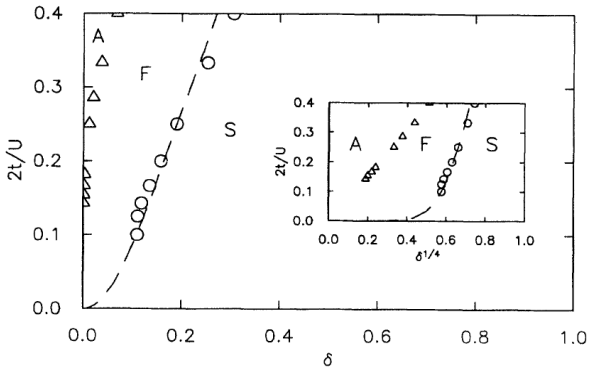


**Fig. 1.1.** Phase diagram in the $2t/U$ versus $\delta$ plane at $T = 0$. Spiral (S), ferromagnetic (F), and antiferromagnetic (A) regions are indicated. The inset shows the behavior near $\delta = 0$.

where $c_{i\sigma} = \sum_{\boldsymbol{k}} e^{i\mathbf{k}\mathbf{R}_i} c_{\boldsymbol{k}\sigma}$ and $\mathbf{R}_i$ is the lattice vector at site $i$. In terms of SRI slave boson operators $H$ may be represented as

$$H = \sum_{\boldsymbol{k}\sigma} \varepsilon_{\boldsymbol{k}} c^\dagger_{\boldsymbol{k}\sigma} c_{\boldsymbol{k}\sigma} + \varepsilon_a \sum_i (\sum_\mu p^\dagger_{i\mu} p_{i\mu} + 2 d^\dagger_i d_i) + V \sum_{i,\sigma,\sigma'} \left( c^\dagger_{i\sigma} z_{i\sigma'\sigma} f_{i\sigma'} + h.c. \right)$$
$$+ U \sum_i d^\dagger_i d_i + \sum_i \{ \alpha_i (Q_b - 1) + \beta_{i0} Q_f + \beta_i \cdot \mathbf{Q}_s \} \tag{1.54}$$

A mean-field approximation to this Hamiltonian describing spiral magnetic states has been considered in [50]. There the nonmagnetic boson mean-field amplitudes $e, d, p_0$ and Lagrange parameters $\alpha, \beta_0$ have been assumed spatially uniform, while the magnetic parameters $\boldsymbol{p}_i$ and $\boldsymbol{\beta}_i$ were taken to have the spatial dependence of a spiral vector field, $\boldsymbol{p}_i = p(\cos\phi_i, \sin\phi_i, 0)$ and $\boldsymbol{\beta}_i = \beta(\cos\phi_i, \sin\phi_i, 0)$ oriented perpendicular to the $z-$axis in spin space, and $\phi_i = \mathbf{q} \cdot \mathbf{R}_i$. The spatial periodicity characterized by the wave vector $\mathbf{q}$ leads to a coupling of Bloch states at wave vectors $\mathbf{k}$ and $\mathbf{k} + \mathbf{q}$. The energy matrix of the hybridized bands then takes the form

$$\epsilon_{\mathbf{k}} = \begin{pmatrix} \epsilon_{\mathbf{k}} - \mu & V z_+ & 0 & V z_- \\ V z_+ & \epsilon_a + \beta_0 - \mu & V z_- & \beta \\ 0 & V z_- & \epsilon_{\mathbf{k}+\mathbf{q}} - \mu & V z_+ \\ V z_- & \beta & V z_+ & \epsilon_a + \beta_0 - \mu \end{pmatrix} \tag{1.55}$$

where the weight factors $z_{+,-}$ are defined by

$$z_\pm = \frac{e p_+ + d p_-}{\sqrt{1 - d^2 - p_+^2}\sqrt{1 - e^2 - p_-^2}} \pm [p_+ \Leftrightarrow p_-] \tag{1.56}$$

with $p_{+,-} = (p_0 \pm p)/\sqrt{2}$. The mean-field values are determined by requiring that the free energy

$$F = -T \sum_{\boldsymbol{k}\sigma\alpha} \ln\left[1 + \mathrm{e}^{\frac{-E_{\mathbf{k}\sigma\alpha}}{T}}\right] + N_L[Ud^2 - \beta_0(p_0^2 + p^2 + 2d^2) + 2\beta p_0 p] \quad (1.57)$$

be stationary. Here $E_{\mathbf{k}\sigma\alpha}$ are the eigenvalues of the energy matrix $\epsilon_{\mathbf{k}}$.

In Fig. 1.1 the zero temperature phase diagram is shown in the $(t/U) - \delta$-plane ($t$ nearest neighbor hopping amplitude, $\delta$ filling factor of the conduction band). In a wide region a spiral magnetic state is found, with wave vector $\mathbf{q}$ approaching the edge of the Brillouin zone at $\delta = 1$ (antiferromagnetic order). Approaching the limit $\delta = 0$ one finds a ferromagnetic region, followed by another antiferromagnetic state very close to $\delta = 0$. These findings have been confirmed by Quantum Monte Carlo simulations [51]. One should keep in mind that the spatial dimension enters only through the energy dispersion of the conduction electrons. These results are therefore applicable in three or higher dimensions, where fluctuation effects are expected to be small.

## 1.4 Fluctuation corrections to the saddle-point approximation: SRI representation of the Hubbard model

Having mapped all degrees of freedom onto bosons allows for directly evaluating the spin and charge response functions. Indeed, the spin and density fluctuations may be expressed as

$$\begin{aligned} \sum_{\sigma} \sigma \delta n_{\sigma} &= \delta(p_0^{\dagger} p_3 + p_3^{\dagger} p_0) \equiv \delta S \\ \sum_{\sigma} \delta n_{\sigma} &= \delta(d^{\dagger} d - e^{\dagger} e) \equiv \delta N \,, \end{aligned} \quad (1.58)$$

in the SRI representation. The spin and charge autocorrelation functions can be written in terms of the slave boson correlation functions as:

$$\begin{aligned} \chi_s(k) &= \textstyle\sum_{\sigma,\sigma'} \sigma\sigma' \langle \delta n_{\sigma}(-k) \delta n_{\sigma'}(k) \rangle = \langle \delta S(-k) \delta S(k) \rangle \\ \chi_c(k) &= \textstyle\sum_{\sigma\sigma'} \langle \delta n_{\sigma}(-k) \delta n_{\sigma'}(k) \rangle = \langle \delta N(-k) \delta N(k) \rangle \quad . \end{aligned} \quad (1.59)$$

Performing the calculation to one-loop order, one can make use of the propagators given in the appendix of Ref. [32] to obtain:

$$\begin{aligned} \chi_s(k) &= 2p_0^2 S_{77}^{-1}(k) \\ \chi_c(k) &= 2e^2 S_{11} S^{-1}(k) - 4ed S_{12}^{-1}(k) + 2d^2 S_{22}^{-1}(k) \,. \end{aligned} \quad (1.60)$$

As emphasized and analyzed by several authors, see e. g. [52,53], a Fermi liquid behavior is obtained when considering the above $\chi_s(k)$ and $\chi_c(k)$ in the long wavelength and low frequency limit. However, in contrast to the conventional

RPA results, the obtained Landau parameters involve effective interactions, which differ in the spin channel and in the charge channel. Performing the algebra at half-filling yields:

$$F_0^a = -1 + \frac{1}{(1+U/U_0)^2}$$
$$F_0^s = \frac{U(2U_0-U)}{(U_0-U)^2} \tag{1.61}$$

fulfilling the property $F_0^s(U) = F_0^a(-U)$ that can be derived on a more general ground [47]. As can be seen in Eq. 1.61 $F_0^a$ remains finite when reaching the Mott transition, while $F_0^s$ diverges (for a recent manifestation of a related behavior see [54]).

Ferromagnetic instabilities and ferromagnetic phases have been investigated, too. In particular, in the limit $U \to \infty$, it could be shown analytically that the fully polarized ferromagnetic ground state and the paramagnetic ground state are degenerate at density $n = 2/3$, for any bi-partite lattice [33]. For lower densities the ground state is paramagnetic.

Yet, in such an analysis, focus is put on a ferromagnetic instability only, while other commensurate or even incommensurate instabilities should be considered as well. This analysis has been carried out by two of us for the Hubbard model on the square lattice [55]. Off half-filling it turned out that the leading instabilities are systematically towards incommensurate states characterized by a wave-vector $(Q_x, \pi)$ for $U < 57\ t$ with $Q_x$ smoothly varying from $\pi$ for $U = 0^+$ down to 0 for $U = 57\ t$. For larger $U$ the wave-vector characterizing the instability is rather of the form $(0, Q_y)$, with $Q_y \simeq \pi$.

Charge instabilities have been looked for as well, in particular through the computation of the charge structure factor [32], though with a negative result even for the t-t'-U repulsive Hubbard model [56]. Instead, the charge

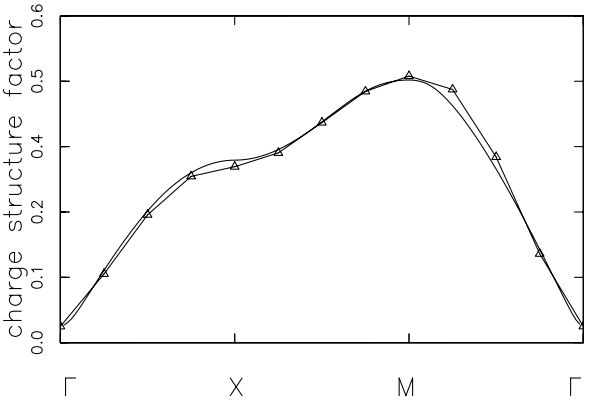


**Fig. 1.2.** Comparison of the Quantum Monte Carlo (triangles) and Slave Boson (full line) charge structure factors for $U = 4t$, $\delta = 0.275$ and $\beta = 6$.

structure factor quite systematically consists of one broad peak centered at $(\pi, \pi)$. As an example we compare in Fig. 1.2 the slave boson result with Quantum Monte Carlo simulations by Dzierzawa [57], for $U = 4t$ and $\delta = 0.275$ at temperature $T = t/6$. The agreement between both approaches is excellent, as the difference does not exceed a few percent.

### 1.4.1 Magnetic and stripe phases

Having established that the leading instabilities of the paramagnetic phase are generically towards incommensurate phases, spiral and stripe phases have been thoroughly investigated [33–39, 45]. Comparison of ground state energies in spiral phases with numerical simulations showed very good agreement [34, 36]. Regarding the pure Hubbard model it has been obtained that magnetic

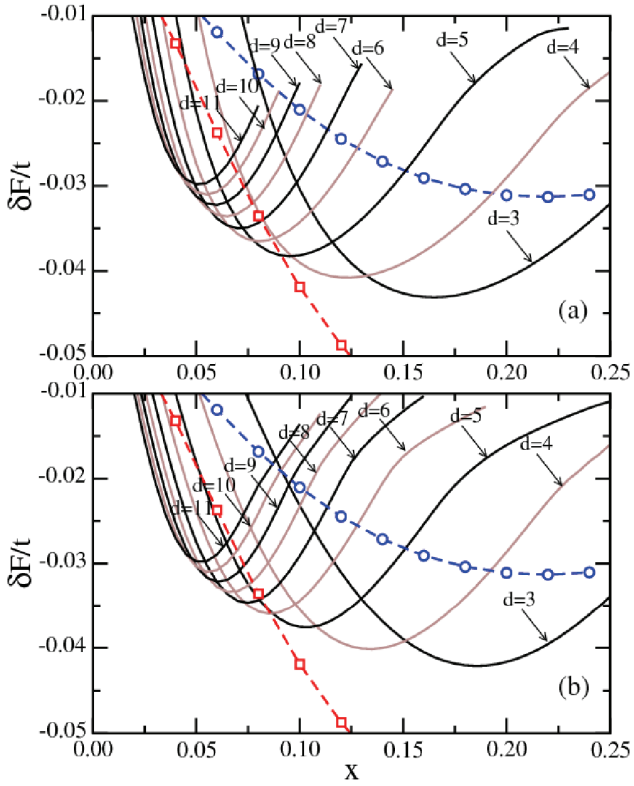


**Fig. 1.3.** Free energy gain $\delta F$ per site with respect to the AF phase as a function of doping $x$, obtained for the $t$-$t'$-$U$ Hubbard Model with $U = 12t$ and $t' = -0.3t$ for: (a) Vertical site-centered stripe phases; (b) vertical bond-centered stripe phases. Domain walls are separated by $d = 3, \ldots, 11$ lattice constants. Circles and squares show the corresponding data for vertical and diagonal spiral order, respectively.

stripe phases are generically more stable than spiral phases. However, for the t-t'-U repulsive Hubbard model, the situation is more intricate. As shown in Fig. 1.3 for an intermediate value of $t'$, a large number of phases compete. While the vertical site-centered stripe phases are generically lower in energy than the vertical bond-centered stripe phases at low doping $x$, the opposite result is found at larger $x$. For instance, for $U = 12t$, the transition occurs at $x \simeq 0.16$ for $t' = -0.15t$, and at $x \simeq 0.18$ for $t' = -0.3t$. Yet, in the latter case, the diagonal spiral phase is lower in energy for $x \geq 0.09$, in contrast to the former case [39].

## 1.5 Conserving self-consistent approximations

### General properties

The KR representation and its SRI and spin-charge symmetric extensions have been remarkably successful in identifying and describing zero-temperature phases of correlated electron models within saddle-point and Gaussian approximations. However, in order to describe dynamical properties, like spectra or non-equilibrium transport, a more accurate treatment of the excitations is needed. This is especially important for understanding Fermi liquid or non-Fermi liquid signatures in these quantities. It requires, in particular, avoiding the spurious condensation transition of the auxiliary boson fields at finite temperature or energy. That is, the auxiliary fields must be treated as pure fluctuation fields, preserving the local $U(1)$ gauge symmetries associated with the conservation of the local constraint charges, Eqs. 1.7, 1.13–1.14, or 1.17–1.19 for the Barnes, the KR, and the SRI representation, respectively. Gauge symmetric theories may be systematically constructed by means of conserving approximations [58], where all irreducible n-point vertex functions are derived from a generating functional $\Phi$ by means of appropriate functional derivatives. This implies that these quantities are calculated self-consistently, i.e., as functionals of the fully renormalized auxiliary particle propagators. Physical expectation values, calculated at first in the grand canonical ensemble of the auxiliary particle occupation numbers utilizing Wick's theorem, are projected onto the physical sector of Fock space at the end of the calculation, using the techniques described in section 1.2.2. In order to capture the correct low-energy properties of a given correlated electron model, the approximation for the generating functional must still be chosen appropriately. The conserving scheme has been extensively pursued within the Barnes representation, in order to keep the number of fluctuating auxiliary fields minimal.

### Exact infrared properties of pseudoparticle propagators

The Fermi or non-Fermi liquid behavior is governed by the infrared asymptotics of the slave boson and pseudofermion propagators, $G_e(\omega)$, $G_d(\omega)$, and

$G_{f\sigma}(\omega)$. By definition, the field operators appearing in these propagators create an impurity site which is initially empty, doubly occupied or singly occupied with spin $\sigma = \pm 1/2$, respectively, and which evolves in time to a final occupation number $n_a = \sum_\sigma n_{a\sigma}$. This process constitutes an orthogonality catastrophy [59] with characteristic infrared powerlaw singularities of the auxiliary particle spectral functions. In the case of a Fermi liquid, the infrared powerlaw exponents of the pseudofermion, empty and doubly occupied slave boson spectral functions, $\alpha_f$, $\alpha_e$, $\alpha_d$, respectively, are determined by the single-particle scattering phase shifts at the Fermi level, which may in turn be expressed in terms of the impurity occupation number $n_a$ via the Friedel sum rule. The dependence of the infrared exponents on $n_a$ is, therefore, an indicator of Fermi liquid or non-Fermi liquid behavior in a given system. For the single-channel Anderson model, Eq. 1.5, which has a Fermi liquid strong-coupling fixed point, one obtains in the absence of a magnetic field [60–62],

$$\alpha_{f\sigma} = n_a - n_a^2/2 \tag{1.62}$$

$$\alpha_e = 1 - n_a^2/2 \tag{1.63}$$

$$\alpha_d = -1 + 2n_a - n_a^2/2 \ . \tag{1.64}$$

These expressions have been confirmed by direct numerical renormalization group calculations [63] and should be recovered by any approximation that is to describe a Fermi liquid fixed point.

### Fock space projection in saddle-point approximation

While the projection onto the physical Fock space with local charge $Q = 1$ (Eq. 1.8) may easily be performed exactly for a single correlated site, it becomes cumbersome already for two sites, let alone for a lattice of correlated electrons. This is because by the exact projection the partition function, for instance, is transformed into the expectation value of the *product* of all the local charges $Q_j$ on the correlated lattice sites $j$ (compare the discussion after Eq. 1.9), i.e., it becomes an $N_L$-point correlation function, where $N_L$ is the number of correlated sites.

However, gauge symmetric, conserving approximations, which avoid any spurious condensate amplitudes and, hence, preserve the infrared properties, can still be constructed when the Fock space projection is done in an approximate way. In this approach, first proposed in [23], the $\lambda$-integration of Eq. 1.8 is done in saddle-point approximation, while all auxiliary particle Green's functions are derived as pure fluctuation propagators from a generating Luttinger-Ward functional. The $\lambda$ saddle point can be shown to be equivalent to fixing $i\lambda$ as a real chemical potential for the thermodynamic average of the local charge, $\langle Q \rangle$. Spurious slave boson condensation is avoided by the fact that the fluctuation part of the Bose propagator acquires finite, *negative* spectral weight $A_{e,d}(\omega) \leq 0$ for negative frequencies, $\omega < 0$, such that the occupation number density, $b(\omega)\ A_{e,d}(\omega)$, remains non-negative for all

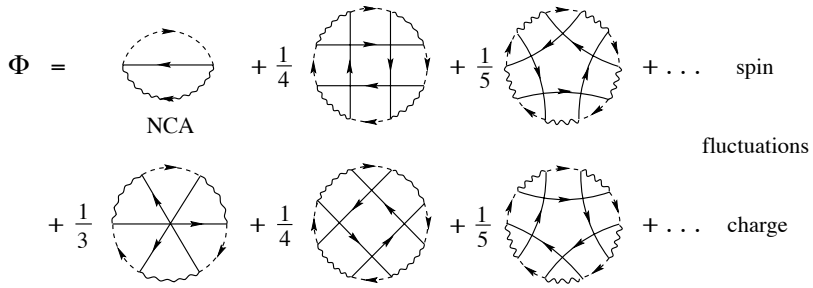


**Fig. 1.4.** Diagrammatic representation of the Luttinger-Ward functional generating the CTMA for $U \to \infty$. The first diagram constitutes the NCA. The two-loop diagram is excluded, since it is not a skeleton. Solid, dashed, and wiggly lines represent conduction electron, renormalized pseudofermion and auxiliary boson propagators, respectively. The terms with the conduction electron lines running clockwise generate the conduction electron-pseudofermion ladder vertex $T^{(cf)}$ with bosons as rungs (spin fluctuations), while the terms with the conduction electron lines running counter-clockwise generate the conduction electron-empty orbital ladder vertex $T^{(ce)}$ with pseudofermions as rungs (charge fluctuations).

$\omega$ [23], with $b(\omega) = 1/(\mathrm{e}^{\beta\omega} - 1)$ the Bose-Einstein distribution. The structure of the self-consistent integral equations for the pseudoparticle propagators is not altered by this approximation. In fact, it may be shown explicitly and in a straight-forward way along the lines of Ref. [64] that the $\lambda$ saddle-point projection preserves the infrared exponents on the level of the simplest conserving approximation, the non-crossing approximation (to be discussed in the next section). It may be conjectured that this remains true also for more sophisticated conserving approximations. Since the $\lambda$ saddle-point approximation involves only the thermal average $\langle Q \rangle$, it is straight-forwardly generalized to lattice problems, with a spatially homogeneous chemical potential $i\lambda \in \mathbb{R}$. The method has been applied to the Heisenberg lattice in pseudofermion representation in Ref. [65].

### 1.5.1 Non-crossing approximation (NCA)

The rest of this chapter is concentrated on the Anderson impurity model.

#### Anderson impurity model for $U \to \infty$: NCA

The simplest conserving approximation in the limit $U \to \infty$ is obtained by choosing the generating functional to lowest, i.e., 2nd order in the hybridization $V$, as shown as the first diagram of Fig. 1.5. Since the self-energies generated in this approximation do not contain any crossings of lines, it has been termed "non-crossing approximation" (NCA). The NCA has been pioneered by Keiter and Kimball using the resolvent operator formalism [66, 67] and by

Kuramoto, who first recognized the conserving nature of the NCA [68]. First numerical evaluations were performed by Kojima et al. [69] and by Bickers [70]. For an efficient and numerically stable algorithm for solving pseudoparticle integral equations, like the NCA and its extensions, see Ref. [71].

For $U \to \infty$ the NCA captures correctly the Kondo energy scale, and it provides a qualitative description of the formation of the Kondo resonance. It happens to describe also correctly the powerlaw dependence of physical properties at the non-Fermi liquid fixed point of the two-channel Anderson or Kondo impurity model [72]. For these reasons and for its technical simplicity the NCA has been applied to a wide variety of problems, including, as an impurity solver for dynamical mean-field theory (DMFT), to the $t-J$ model [73,74] and the non-Fermi liquid two-channel Anderson lattice model [75,76] as well as to phase transitions in dilute, magnetic semiconductors at not too low temperature [77]. The NCA has also been generalized to the case of multiple local orbitals, as in rare earth and transition metal ions, where the NCA correctly produces a distinct Kondo resonance for each crystal-field or spin-orbit split local orbital, each with a characteristic, logarithmic temperature dependence [78,79].

However, in NCA the infrared exponents of the auxiliary particle propagators come out independent of $n_a$, $\alpha_f^{NCA} = 1/(N+1)$, $\alpha_e^{NCA} = N/(N+1)$ [64, 71], with $N$ the spin degeneracy, in contrast to the Fermi liquid values, Eqs. 1.62-1.64. As a consequence, the NCA fails to describe Fermi liquid behavior at temperatures $T \ll T_K$, with spurious infrared singularities appearing in physical quantities at energies or temperatures $T \ll T_K$ [64, 70, 71]. Since the NCA becomes formally exact for SU($N$) symmetric models in the limit $N \to \infty$, with deviations appearing in $O(\frac{1}{N^2})$ [70, 80], this low-$T$ failure is less pronounced for $N \gg 1$. Note, however, that the deviation of the NCA infrared exponents $\alpha_f$, $\alpha_e$ is of order $1/N$, not $1/N^2$ as one may have expected. In a magnetic field the NCA also fails even in the high temperature regime, $T > T_K$, producing a spurious resonance in the impurity spectrum at $\omega = 0$ in addition to the two Zeeman-split Kondo peaks. The low-$T$ failure of the NCA can be traced back to its insufficient inclusion of coherent multiple spin-flip processes which are responsible for the formation of the Kondo singlet state. The origin of the failure in a magnetic field, on the other hand, lies in the fact that NCA neglects the exchange diagram to the conduction electron-impurity spin vertex at 2nd order in the spin coupling $J$ [62,81]. As a consequence, logarithmic contributions in the potential scattering channel do not cancel even in leading logarithmic order, producing a spurious resonance which does not Zeeman-split in a magnetic field.

### Anderson impurity model with finite $U$: SUNCA

At finite Coulomb interaction $U$, the spin exchange interaction $J$ acquires contributions from both, virtual excitations to the empty and to the doubly occupied impurity states via a Schrieffer-Wolff transformation [82],

$$J = \frac{|V|^2}{|\epsilon_f|} + \frac{|V|^2}{|\epsilon_f + U|} \tag{1.65}$$

Neglecting either one of these contributions would lead to an exponentially wrong Kondo scale $T_K$, because of the exponential dependence of $T_K$ on $J$. A simple generalization of NCA to this case, i.e., adding the 2nd order self-consistent perturbation theory for the two processes, fails to capture the simultaneous contribution of both channels in each order of bare perturbation theory. For a correct treatment of both terms, there must be included, for each diagram with an empty boson line $G_e$, the corresponding diagram with $G_e$ replaced by a doubly occupied boson line $G_d$ (which amounts to the exchange diagram of the former), and vice versa, *on the level of bare perturbation theory* [83, 84]. The corresonding vertex corrections have first been evaluated in leading self-consistent order by Sakai et al. [85] and by Pruschke and Grewe [86]. The first conserving approximation for finite $U$, fully symmetric with respect to the empty and double occupied fluctuation channels, was formulated and evaluated by Haule *et al.* [83] and termed as the symmetrized finite-U NCA (SUNCA). On the level of renormalized perturbation theory (generating functionals), it means that for each dressed $b$-line there must be included a ladder vertex function with $a$-lines as rungs, and vice versa. The SUNCA is tractable with relatively moderate numerical effort, since it can be formulated in terms of no higher than 3-point vertex functions. The results of a fully selfconsistent evaluation of the impurity electron spectral function within SUNCA are shown in Fig. 1.5.1 in comparison with NRG results. It is seen that the correct Kondo scale (width of the Kondo peak) is reproduced. However, like the NCA, the SUNCA solution still develops a spurious low-$T$ singularity.

There is evidence that both failures of NCA, at low temperature and in a magnetic field, can be cured by a systematic resummation of coherent spin flip terms to infinite order, which will be discussed in the next section.

### 1.5.2 Conserving T-matrix approximation (CTMA)

#### Construction of the CTMA

As a minimal precondition to obtain a gauge symmetric description of the Fermi liquid fixed point, a conserving approximation must reproduce the correct pseudoparticle infrared exponents, Eqs. 1.62-1.64, whose dependence on $n_a$ is characteristic for a Fermi liquid ground state. It is easily seen by power counting arguments that any summation of a finite number of skeleton self-energy diagrams merely reproduces the incorrect NCA exponents [80], like, e.g., the post-NCA considered by Anders [88] (diagrams up to $\mathrm{O}(\Gamma^4)$ in Fig. 1.5). Hence, the generating functional must be comprised of an *infinite* class of skeleton diagrams in order to describe Fermi liquid behavior. Since the latter is a consequence of the singlet state formed at low $T$ between the impurity

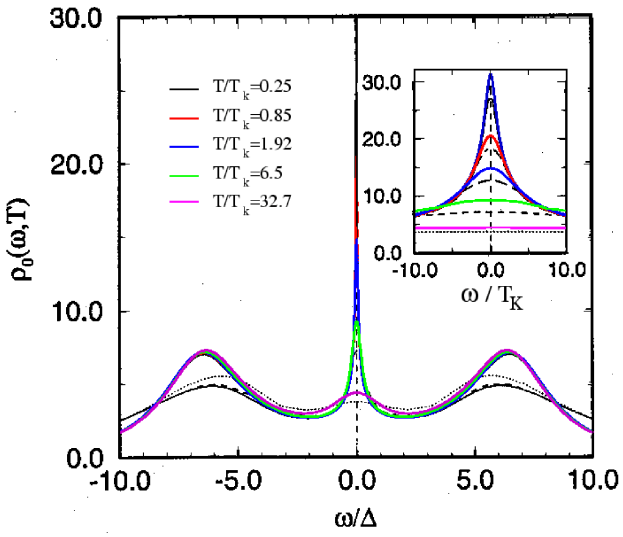


**Fig. 1.5.** Physical impurity electron spectral function of the Anderson impurity model for $U = -2\epsilon_f$. Solid lines: SUNCA results [83], dashed lines: NRG results [87].

and the conduction electron spins, one may expect that higher than two-particle correlation functions need not be considered in the single-channel case. The approximations to the total vertex functions between conduction electons ($c$) and impurity degrees of freedom (pseudofermions $f$, slave bosons $e$) are then two-particle T-matrices, $T^{(cf)}$, $T^{(ce)}$. As the irreducible parts of these T-matrices we select the single (renormalized) $e$ or $f$ particle lines, since (1) in the Kondo regime these terms are the leading contributions in the small parameter $VN_0$; and (2), in the spirit of principal diagrams, this choice gives rise to the maximum number of spin and charge fluctuation processes, respectively, in the T-matrices at any given order of (renormalized) perturbation theory. The Luttinger-Ward functional generating these ladder vertex terms (and others) for $U \to \infty$ is shown in Fig. 1.5. It is comprised of all closed pseudoparticle rings (skeletons) with each conduction electron line spanning at most two hybridization vertices and has been termed the conserving T-matrix approximation (CTMA) [61, 89]. Via the self-consistent inclusion of the self-energies, the vertex equations for $T^{cf}$, $T^{ce}$, have parquet character. The CTMA integral equations, the analytical expressions for the self-energies, $\Sigma_{f\sigma}$, $\Sigma_e$, and the impurity electron Green's function, $G_{a\sigma}$, are given explicitly in Ref. [89, 90]. Keiter and co-workers [91, 92] efficient decoupling scheme for the CTMA integral equations, which greatly facilitates the evaluation, and which preserves the Fermi liquid values of the auxiliary particle infrared exponents.

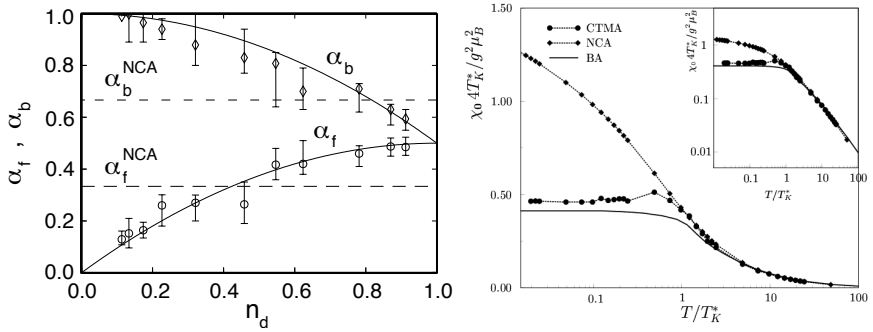


**Fig. 1.6.** Left panel: CTMA results (symbols with error bars) for the threshold exponents $\alpha_f$ and $\alpha_e$ for $U \to \infty$, $B = 0$. Solid lines: Exact values, Eqs. (1.62,1.63), dashed lines: NCA results. Right panel: Static spin susceptibility as a function of temperature; Bethe ansatz, CTMA and NCA results (see text). Model parameters used: $\epsilon_d/D = -0.81$, $\Gamma/D = 0.2$.

## Principal results

*Pseudoparticle spectral functions.* As a first indication for description of Fermi liquid behavior within CTMA it has been checked if the CTMA reproduces the correct Fermi liquid values of the pseudoparticle threshold exponents [61]. The exponents of the CTMA solution are displayed in Fig. 1.5.2 (left panel) and show, within the error bars, good agreement with the exact values, especially the dependence on the impurity occupation number $n_d$, characteristic for the Fermi liquid fixed point.

*The static spin susceptibility* of the impurity was calculated from the spin dependent occupation numbers $n_{a\sigma}$ in a small magnetic field $\mathcal{B}$ as,

$$\chi_i(T) = \left.\frac{dM}{d\mathcal{B}}\right|_{\mathcal{B}=0} \tag{1.66}$$

where $M = g\mu_B \sum_\sigma \sigma n_{a\sigma}$ is the impurity magnetization and

$$n_{a\sigma} = \lim_{\lambda\to\infty} \frac{\int d\omega e^{-\beta\omega}\, \mathrm{Im} G_{f\sigma}(\omega - i0)}{\int d\omega e^{-\beta\omega}\, \mathrm{Im}[\sum_\sigma G_{f\sigma}(\omega - i0) + G_e(\omega - i0)]} \ . \tag{1.67}$$

$\chi_i(T)$ is shown in Fig. 1.5.2 (left panel). It exhibits $T$-independent Pauli behavior for $T \lesssim 0.5 T_K$ with no singular behavior appearing down to the lowest $T$ considered [90], indicative of the Fermi liquid ground state with a completely screened local moment. As expected, $\chi_i(T)$ obeys scaling for at least a range of $T_K$ within a factor 10 [93], when plotted as a function of $T/T_K$. For details of the comparison with the Bethe ansatz results in Fig. 1.5.2 (left panel) see Ref. [90].

Fermi liquid behavior of the impurity electron Green's function

$$G_{a\sigma}(\omega) = [\omega - \epsilon_f - i\Gamma - \Sigma_{a\sigma}(\omega)]^{-1} \ , \tag{1.68}$$

and the impurity electron interaction self-energy $\Sigma_{d\sigma}(\omega)$ is of prime interest especially for applications within DMFT. $\Sigma_{a\sigma}$ exhibits many features of Fermi liquid behavior [90]. It has quadratic dependence on both, $\omega$ and $T$, at low $\omega$, $T$, with no sign of a spurious low-energy singularity down to the lowest $T$ considered ($T \simeq 0.01\ T_K$). As discussed in detail in Ref. [90], the curvature of the quadratic behavior in $\omega$ and $T$ is found to be in good agreement with the exact Fermi liquid result, $\Sigma_{a\sigma}(\omega) = a[\omega^2 + (\pi T)^2]/T_K^2$, where $a$ is an exactly known prefactor. However, the position $\omega_0$ of the minimum of $\mathrm{Im}\Sigma_{a\sigma}(\omega)$ is incorrectly shifted to $\omega_0 \approx -T_K$, and $\mathrm{Im}\Sigma_{a\sigma}(\omega - i0)$ acquires negative values, thus violating the Friedel sum rule. When searching for the origin of this shortcoming, one must keep in mind that $\Sigma_{a\sigma}(\omega \approx 0)$ is determined via Eq. (1.68) by both $\mathrm{Im}G_{a\sigma}(\omega)$ and $\mathrm{Re}G_{a\sigma}(\omega)$, and thus, via the Kramers-Kronig relation, by high-energy (potential scattering) contributions to $G_{a\sigma}(\omega)$. Hence, the erroneous shift $\omega_0$ may result from an unprecise calculation of $G_{a\sigma}(\omega)$ at high energies, either numerically or due to neglect of high-order potential scattering terms [94]. To correct this shortcoming, it has been suggested to add an appropriate, phenomenological *real constant* to $\Sigma_{a\sigma}(\omega)$. Through selfconsistency it acts like a chemical potential and shifts the minimum of $\mathrm{Im}\Sigma_{a\sigma}(\omega)$ to $\omega = 0$. By inclusion of that single, real parameter, motivated by potential scattering contributions, the full Fermi liquid behavior of $\Sigma_{a\sigma}(\omega)$ is recovered, and $G_a(\omega)$ obeys the unitarity sum rule with good precision [90].

## 1.6 Renormalization group approaches

The renormalization group method is a powerful tool to calculate properties of interacting many-body systems. In the context of strongly correlated electron systems a first and seminal application of the method to the Kondo problem has been proposed by P. W. Anderson [95], who coined the term "poor man's scaling" for his method. While Anderson's treatment is perturbative in the exchange coupling constant of the Kondo model, and is therefore valid only at not too low energies, Wilson devised a numerical RG method for the Kondo model which he successfully implemented to cover the complete range of energies [96]. While these early RG formulations were phrased in terms of successive mappings of the Hamiltonian with continuously decreasing band width compensated by correspondingly adjusted coupling constants, the later Functional Renormalization Group (FRG) schemes make use of a mapping of the complete set of Green's functions under a continuous change of an infrared cutoff. For the Kondo model, this is most conveniently formulated using the pseudofermion representation of the local spin 1/2. The "poor man's scaling" approach to the equilibrium Kondo model is essentially a simplified FRG formulation, in which the RG flow of the pseudofermion self energy and the energy dependence of the exchange coupling function, as well as all higher order couplings are neglected. It may be generalized to out of equilibrium

situations, if the self-energy (the imaginary part of which describes the relaxation rate of the local spin) and the energy dependence of the coupling are kept. It is actually even possible to extend the RG approach into the strong coupling regime, provided the effect of the self-energy in controlling the flow of the coupling is treated correctly. Finally, the FRG has been successfully used to treat another strong coupling problem, that of frustrated quantum spin systems on a lattice in pseudofermion representation.

### 1.6.1 "Poor man's scaling" in the equilibrium Kondo model

The interaction of a Fermi sea with a quantum impurity, e.g. a local spin exchange coupled to the local spin density of the Fermi system, gives rise to the Kondo effect. Initially introduced to describe magnetic impurities in metals, the Kondo problem is by now a ubiquitous phenomenon. The corresponding s-d exchange Hamiltonian, or Kondo Hamiltonian for short, reads

$$H = \sum_{\boldsymbol{k}\sigma} \varepsilon_{\boldsymbol{k}} c^\dagger_{\boldsymbol{k}\sigma} c_{\boldsymbol{k}\sigma} + J \sum_{\boldsymbol{k}\boldsymbol{k}'\sigma\sigma'} \frac{1}{2} c^\dagger_{\boldsymbol{k}\sigma} \boldsymbol{\tau}_{\sigma\sigma'} c_{\boldsymbol{k}'\sigma'} \cdot \boldsymbol{S}\,, \tag{1.69}$$

where $\boldsymbol{S} =$ is the local spin 1/2 operator in pseudofermion representation, Eq. 1.1, $J$ is the exchange coupling constant and $\boldsymbol{\tau}_{\sigma\sigma'}$ is the vector of Pauli matrices. We take a flat conduction electron DOS, $N(\omega) = \frac{1}{2D}\theta(D_0 - |\omega|)$. If we now transform this Hamiltonian to an equivalent one with reduced band width $D = D_0 - dD$, the physical properties of the system remain unchanged, provided the exchange coupling is changed correspondingly. In order to calculate the required adjusted value of $J$ at the scale $D$, denoted $J(D)$ one may determine the effective coupling in perturbation theory in $J$. The lowest (second order in $J$) correction terms $\delta J$ are shown in Fig. 1.6.1, where the dashed (solid) lines depict bare retarded pseudofermion (local Keldysh conduction electron) Green's functions. Differentiating $\delta J$ with respect to the running band width $D$ one finds that in lowest order in the dimensionless coupling constant $g_0 = N(0)J$ the renormalized coupling $g(D)$ obeys the RG equation [95]

$$\frac{dg(D)}{d\ln D} = -2g^2 + O(g^3) \tag{1.70}$$

with the solution

$$g(D) = \frac{1}{2\ln(D/T_K)} \tag{1.71}$$

where $T_K = D_0 \exp(-1/2g_0)$ is the Kondo temperature. One observes that $g(D)$ diverges at $D = T_K$. The divergence is removed by taking the pseudofermion self-energy into account, the imaginary part of which describes the relaxation rate for spin flip processes (see below). The above perturbative RG

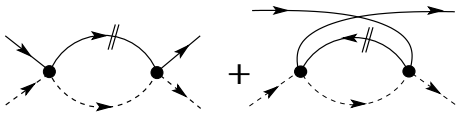

**Fig. 1.7.** Diagrammatic representation of the RG vertex in 2nd order of $J$. The strokes indicate differentials with respect to the band cutoff D. Dashed and solid lines depict bare retarded pseudofermion and local Keldysh conduction electron Green's functions, respectively.

result provides a valid description as long as the running coupling is small, $g(D) << 1$. In the perturbative regime the Kondo effect, i.e. the screening of the local spin by the conduction electron spins, begins to build up. The screening is completed at the energy or temperature scale $T << T_K$, i.e. in the strong coupling regime, not accessible by perturbative methods.

### 1.6.2 Functional RG for the Kondo model out of equilibrium

The Kondo problem experienced a revival in the mid 1990s, when it was found that charge transport through nano structures may be dominated by the Kondo effect, in the sense that the Kondo resonance at a quantum dot may lead to perfect conductance through the dot, although it is only weakly coupled to the leads [97,98]. The corresponding Kondo Hamiltonian of a local spin exchange-coupled to the conduction electron spin densities in the two leads at the dot and the transfer operator through the dot reads,

$$H = \sum_{\boldsymbol{k}\sigma\alpha} (\varepsilon_{\boldsymbol{k}} - \mu_\alpha) c^\dagger_{\boldsymbol{k}\sigma\alpha} c_{\boldsymbol{k}\sigma\alpha} + \sum_{\boldsymbol{k}\boldsymbol{k}'\sigma\sigma'} J_{\alpha\alpha'} \frac{1}{2} c^\dagger_{\boldsymbol{k}\sigma\alpha} \boldsymbol{\tau}_{\sigma\sigma'} c_{\boldsymbol{k}'\sigma'\alpha'} \cdot \boldsymbol{S} \tag{1.72}$$

where $\alpha = L, R$ labels the leads and $\mu_\alpha = \pm eV/2$ denotes the chemical potential shifts in the leads induced by an applied d.c. bias voltage $V$. In the following the matrix of exchange couplings is assumed isotropic ($J_{\alpha\alpha'} = J$).

As first proposed in [99–102], and later derived within a full functional RG treatment [103], the "poor man's scaling" approach may be generalized to non-equilibrium by keeping the energy dependence of the coupling function $g(\omega) = J(\omega)N(0)$ and by observing that the RG flow is cut off at the scale of the spin relaxation rate $\Gamma$. The role of $\Gamma$ in suppressing the Kondo effect has been demonstrated within NCA in [104]. The generalized RG equation may be formulated as

$$\frac{dg(D;\omega)}{d\ln D} = -\sum_{\alpha=\pm} g^2(D;\alpha eV/2)\theta(D - \sqrt{(\omega + \alpha eV/2)^2 + \Gamma^2}) \tag{1.73}$$

This equation must be solved simultaneously with the relaxation rate at scale $D$

$$\Gamma = \pi \sum_{\alpha=L,R} \int d\omega g^2(D;\omega) f(\omega - \mu_\alpha)[1 - f(\omega - \mu_{\alpha'})] \tag{1.74}$$

where $f(\omega)$ is the Fermi function of the conduction electrons. The charge current is given by the expression

$$I = e\frac{3\pi}{4} \int d\omega g^2(D;\omega)\{f(\omega - \mu_L)[1 - f(\omega - \mu_R)] - (L \Leftrightarrow R)\} \tag{1.75}$$

Excellent agreement of the above theory with experimental data is found provided the bias voltage, the applied magnetic field (Zeeman splitting $B$) or temperature is sufficiently high, $eV, B, T >> T_K$ so that the perturbative expression of the RG $\beta$-function is applicable [99, 100, 105–110].

### 1.6.3 RG approach to the Kondo model at strong coupling

Motivated by the success of the generalized RG in non-equilibrium and the insights gained from there, one may ask whether that formulation may be extended to the strong coupling domain. This has been attempted back in the 1970s by U. Larsen and R. Mattuck (LM) [111], who discovered that the weak coupling RG equation, combined with the cutoff $\Gamma$ provided by the relaxation rate shifts the singularity in $g(D)$ from $D = T_K$ down to $D = 0$. In the limit $T \to 0$ the relaxation rate $\Gamma$ was found to approach the value $T_K$, the exchange coupling developed the singular behavior $g(T) \propto 1/T$ and the conductance assumed the exact unitarity limit. It is worth noting that LM employed the pseudofermion representation with particle-hole symmetric projection. The flaw in LM's derivation was that the leading low temperature corrections turned out to be linear in $T$ instead of quadratic, as required by Fermi liquid theory. This difficulty has been recently resolved by using the correct form of the RG $\beta$-function in the strong coupling regime [112]. In addition, it may be shown that while LM considered only the lowest (single particle-hole excitation) contribution to $\Gamma$, all the higher order contributions may be subsummed to give the same structure, but with modified numerical coefficients. As shown in [112] the $\beta$-function in the strong coupling regime grows as $g^3$, and therefore faster than in the weak coupling limit. A useful interpolation expression is

$$\frac{dg(D)}{d\ln D} = -\frac{[g(2+g)]^2}{2+2g}\theta(D - \Gamma) \tag{1.76}$$

This equation may be solved analytically to give

$$g(D) = \sqrt{1 + 1/\ln(\sqrt{D^2 + \Gamma^2}/T_K)} - 1 \tag{1.77}$$

where $T_K$ has been defined above. Here the relaxation rate is given by the self-consistent equation

$$\Gamma(T) = 3g^2(T) \int d\omega d\omega' f(\omega') f(\omega - \omega') f(-\omega) \frac{\Gamma}{\omega^2 + \Gamma^2} \tag{1.78}$$

where $f(\omega)$ denotes the Fermi functions of both, conduction electrons and pseudofermions. At temperatures $T \ll \Gamma$ the integral may be evaluated to give $\Gamma^2(T) = c_\Sigma g^2(T) T^2$ ($c_\Sigma = 3\pi^2/4$ ), which when combined with Eq.(69) results in a finite value of the relaxation rate, $\Gamma = T_K + c_\Gamma T^2/T_K + O(T^3)$ ($c_\Gamma = c_\Sigma - 1/2$ ) and a diverging coupling $g(T) = c_g/T$. The conductance $G$ through a Kondo dot in the linear response regime is given by

$$\frac{G}{G_0} = 3g^2 Y \int d\omega d\omega' f(\omega') f(\omega - \omega') f(-\omega) \frac{\Gamma}{\omega^2 + \Gamma^2} \frac{\Gamma}{(\omega')^2 + \Gamma^2} \tag{1.79}$$

where $G_0$ is the conductance quantum and $Y$ is the correction factor introduced in the section on particle-hole symmetric projection above ($Y \to 1$ as $T \to 0$). One observes that $G/G_0 \to 1$ as $T \to 0$ (unitarity).

### 1.6.4 Functional RG approach to frustrated Heisenberg models

The pseudofermion representation of spin operators may also be used in lattice models. Here again the p-h symmetric projection is useful, particularly when one is interested in the low temperature behavior ($T \ll J$). The more conventional approximation schemes (random phase approximation, FLEX approximation) when applied to the Heisenberg model on the square lattice have been shown to provide good results [65]. The effect of the exact projection via Popov-Fedotov has been found to be only important at higher temperatures, as expected [19]. Systems of recent interest are frustrated Heisenberg models, with competing interactions. Any approximate treatment should be carefully balanced as to not prefer one type of correlations over another one. A systematic treatment of all interaction channels may be achieved by employing the functional RG method [113–115]. A first study of a frustrated Heisenberg model at $T = 0$ using the pseudofermion representation and the FRG method provided excellent results on the phase diagram of the $J_1 - J_2$-model [22]. Similar to the treatment of the Kondo model by FRG mentioned above, one keeps only the two first RG-equations out of the infinite hierarchy of equations. It is necessary to keep the full energy dependence of self-energy and two-particle vertex functions. In addition, it turns out to be important to keep a three-particle correlation contribution in the form of self-energy insertions in the $\beta$-function of the RG equation for the couplings [116]. In this way the Ward identities may be approximately satisfied. While this method cannot yet be used to calculate properties of the ordered state, it allows to identify phases without long-range order by studying whether the RG flow runs smoothly all the way to $\Lambda = 0$ ($\Lambda$ is the infrared cut off parameter of FRG), which indicates a phase without LRO, or whether the flow becomes

unstable at some finite $\Lambda$ , pointing to the existence of LRO. A recent application to the $J_1 - J_2 - J_3$-model yielded again excellent agreement with complementary methods [117].

## 1.7 Conclusion

We have reviewed the most prominent auxiliary particle techniques and their applications to strongly correlated electron systems, using a variaty of approximation schemes, ranging from saddle-point approximations, possibly with Gaussian fluctuations, to conserving approximations to renormalization group methods. It was seen that the Kotliar-Ruckenstein representation, especially in its spin rotation invariant and spin-charge symmetric formulation, is particularly useful for identifying complex spin and/or charge ordered groundstates in mean-field like approximations, since it treats all spin and charge states on a lattice site on the same footing. Regarding the Hubbard model on the square lattice, unrestricted Hartree-Fock calculations point towards a huge number of solutions. An indication that this is also realized using slave bosons on the saddle-point level is provided by Fig. 1.3, but identifying the numerous competing phases remains a challenge. Conserving approximations provide a versatile tool for implementing the constraint on the auxiliary particle number and, hence, for a thorough treatment of fluctuations without resorting to a mean-field as a starting point. This appears necessary in particular for quantum impurity systems, where magnetic ordering does not occur. The NCA and the CTMA have been discussed as the most prominent examples of this approach. Finally, Larsen's particle-hole symmetric projection technique may provide a promising tool for describing the complete RG flow from the weak coupling regime to the strong coupling fixed point within a diagrammatic RG.

### Acknowledgments

We thank Jan Brinckmann, Theo Costi, Klaus Doll, Michael Dzierzawa, Peter Hirschfeld, Stefan Kirchner, Thilo Kopp, Gabi Kotliar, Burkhart Möller, Kandkher Muttalib, Andrzej Oleś, Henni Ouerdane, Jens Paaske, Marcin Raczkowski, Johannes Reuther, Achim Rosch, Holger Schmidt, and Walter Zimmermann for valuable collaboration. RF gratefully acknowledges financial support by the Région Basse-Normandie and the Ministère de la Recherche. JK is grateful for financial support from the Deutsche Forschungsgemeinschaft through SFB 608 and through grant No. KR 1727/1-2 and PW acknowledges support through the DFG Research Center for Functional Nanostructures (CFN).

## References

1. M. Imada, A. Fujimori, and Y. Tokura, Rev. Mod. Phys. **70**, 1039 (1998)

2. P. A. Lee, T. M. Rice, J. Serene, L. J. Sham and J. W. Wilkins, Comments on Condensed Matter Physics, **12,** 99 (1986)
3. P. W. Anderson, Science **235,** 1196 (1987)
4. A. C. Hewson, "The Kondo Problem to Heavy Fermions" (Cambridge University Press, (1993)
5. T. Holstein and H. Primakoff, Phys. Rev. **58,** 1094 (1940)
6. J. Schwinger, "Quantum Theory of Angular Momentum", eds. H. Biedenharn and H. Van Dam (Academic, New York, 1965)
7. A. A. Abrikosov, Physics (Long Island City, N.Y.) **2**, 5 (1965)
8. B. Coqblin and J. R. Schrieffer, Phys. Rev. **185**, 847 (1969)
9. S. E. Barnes, J. Phys. F **6**, 1375 (1976); **7**, 2637 (1977)
10. P. Coleman, Phys. Rev. B **29**, 3035 (1984)
11. M. Gutzwiller, Phys. Rev. Lett. **10**, 159 (1963)
12. G. Kotliar and A.E. Ruckenstein, Phys. Rev. Lett. **57**, 1362 (1986)
13. T.C. Li, P. Wölfle, and P.J. Hirschfeld, Phys. Rev. B **40**, 6817 (1989)
14. R. Frésard and P. Wölfle, Int. J. of Mod. Phys. B **6**, 685 (1992), Int. J. of Mod. Phys. B **6**, 3087 (1992)
15. R. Frésard and G. Kotliar, Phys. Rev. B **56**, 12 909 (1997)
16. F. Lechermann, A. Georges, G. Kotliar, and O. Parcollet, Phys. Rev. B **76**, 155102 (2007)
17. U. Larsen, Z. Physik **256**, 65 (1972)
18. V. N. Popov and S. A. Fedotov, Sov. Phys. JETP **67**, 535 (1988)
19. J. Brinckmann and P. Wölfle, Physica B **359-361**, 798 (2005)
20. M. N. Kiselev and R. Oppermann, JETP Lett. **71**, 250 (2000)
21. R. Dillenschneider and J. Richert, Phys. Rev. B **73**, 024409 (2006)
22. J. Reuther and P. Wölfle, Phys. Rev. B **81**, 144410 (2010)
23. J. Kroha, P. Hirschfeld, K. A. Muttalib, and P. Wölfle Solid State Comm. 83 (12), 1003 (1992)
24. N. Read, D. M. Newns, J. Phys. C **16**, L1055 (1983); *ibid.* 3273 (1983); D. M. Newns and N. Read, Adv. in Physics **36,** 799 (1987)
25. R. Frésard and T. Kopp, Nucl. Phys. B **594**, 769 (2001)
26. R. Frésard, H. Ouerdane, and T. Kopp, Nucl. Phys. B **785**, 286 (2007)
27. J.W. Rasul, T. Li, J. Phys. C **21**, 5119 (1988); T.C. Li and J.W. Rasul, Phys. Rev. B **39**, 4630 (1989); J.W. Rasul, T.C. Li and H. Beck, Phys. Rev. B **39**, 4191 (1989)
28. M. Lavagna, Phys. Rev. B **41**, 142 (1990); Helvetica Physica Acta **63**, 310 (1990); Int. J. Mod. Phys. B **5**, 885 (1991)
29. Th. Jolicœur and J.C. Le Guillou, Phys. Rev. B **44**, 2403 (1991)
30. Y. Bang, C. Castellani, M. Grilli, G. Kotliar, R. Raimondi and Z. Wang, Int. J. of Mod. Phys. B **6**, 531 (1992)
31. R. Frésard and T. Kopp, Phys. Rev. B. **78**, 073108 (2008)
32. W. Zimmermann, R. Frésard, and P. Wölfle, Phys. Rev. B **56**, 10 097 (1997)
33. B. Möller, K. Doll, and R. Frésard, J. Phys. Condensed Matter **5** 4847 (1993)
34. R. Frésard, M. Dzierzawa and P. Wölfle, Europhys. Lett. **15**, 325 (1991)
35. E. Arrigoni and G. C. Strinati, Phys. Rev. B **44**, 7455 (1991)
36. R. Frésard and P. Wölfle, J. Phys. Condensed Matter **4** 3625 (1992)
37. G. Seibold, E. Sigmund, and V. Hizhnyakov, Phys. Rev. B **57**, 6937 (1998)
38. M. Raczkowski, R. Frésard, and A. M. Oleś, Phys. Rev. B **73**, 174525 (2006)
39. M. Raczkowski, R. Frésard, and A. M. Oleś, Europhys. Lett. **76**, 128 (2006)

40. A. Isidori and M. Capone, Phys. Rev. B **80**, 115120 (2009)
41. A. Ruegg, S. Pilgram, and M. Sigrist, Phys. Rev. B **75**, 195117 (2007)
42. P. Korbel, W. Wojcik, A. Klejnberg, J. Spałek, M. Acquarone, and M. Lavagna, Eur. Phys. J. B, **32**, 315 (2003)
43. G. Kotliar, E. Lange, and M. J. Rozenberg, Phys. Rev. Lett. **84**, 5180 (2000)
44. G. Seibold, Phys. Rev. B **58**, 15520 (1998)
45. J. Lorenzana and G. Seibold, Low Temp. Phys. **32**, 320 (2006)
46. W. F. Brinkman and T. M. Rice, Phys. Rev. B. **2**, 4302 (1970)
47. D. Vollhardt, Rev. Mod. Phys. **56**, 99 (1984); D. Vollhardt, P. Wölfle, and P. W. Anderson, Phys. Rev. B. **35**, 6703 (1987)
48. S. Doniach, Physica B&C **91**, 231 (1977)
49. H. v. Löhneysen, A. Rosch, M. Vojta and P. Wölfle, Rev. Mod. Phys. **79**, 1015 (2007)
50. B. Möller and P. Wölfle, Phys. Rev. B **48**, 10320 (1993)
51. M. Guerrero and R. M. Noack, Phys. Rev. B **53**, 3707 (1996)
52. T.C. Li, Y.S. Sun and P. Wölfle, Z. Phys. B - Condensed Matter **82**, 369 (1991)
53. T.C. Li and P. Bénard, Phys. Rev. B. **50**, 17 387 (1994)
54. P. Limelette, H. Muguerra, and S. Hébert, Phys. Rev. B **82**, 035123 (2010)
55. K. Doll, M. Dzierzawa, R. Frésard, and P. Wölfle, Z. Phys. B - Condensed Matter **90**, 297 (1993)
56. R. Frésard and W. Zimmermann, Phys. Rev. B **58**, 15288 (1998)
57. M. Dzierzawa, unpublished.
58. G. Baym and L. P. Kadanoff, Phys. Rev. **124** (1961) 287; G. Baym, Phys. Rev. **127**, 1391 (1962)
59. P. W. Anderson, Phys. Rev. Lett. **18**, 1049 (1967); Phys. Rev. **164**, 352 (1967)
60. B. Menge and E. Müller-Hartmann, Z. Phys. B **73**, 225 (1988)
61. J. Kroha and P. Wölfle, T.A. Costi, Phys. Rev. Lett. **79**, 261 (1997)
62. J. Kroha and P. Wölfle, J. Phys. Soc. Jpn. **74** (1), 16 (2005)
63. T.A. Costi, P. Schmitteckert, J. Kroha and P. Wölfle, Phys. Rev. Lett. **73**, 1275 (1994); Physica **C235-240** (1994) 2287.
64. E. Müller-Hartmann: Z. Physik **B 57**, 281 (1984); Y. Kuramoto, E. Müller-Hartmann: J. Mag. Mag. Mat. **52**, 122 (1985)
65. J. Brinckmann and P. Wölfle, Phys. Rev. B **70**, 174445 (2004)
66. H. Keiter, J.C. Kimball, Int. J. Magn. **1** 233 (1971)
67. N. Grewe and H. Keiter, Phys. Rev. B **24** 4420 (1981)
68. Y. Kuramoto, Z. Physik B **53**, 37 (1983)
69. H. Kojima, Y. Kuramoto, and M. Tachiki, Z. Physik **B 54**, 293 (1984); Y. Kuramoto, H. Kojima, Z. Physik **57**, 95 (1984); Y. Kuramoto: Z. Physik **B 65**, 29 (1986)
70. N.E. Bickers, D.L. Cox, and J. W. Wilkins, Phys. Rev. **B 36**, 2036 (1987); N.E. Bickers, Rev. Mod. Phys. **59**, 845 (1987)
71. T.A. Costi, J. Kroha, and P. Wölfle, Phys. Rev. **B 53**, 1850 (1996)
72. P. Nozières and A. Blandin, J. Phys. (Paris) **41**, 193 (1980)
73. K. Haule, A. Rosch, J. Kroha, P. Wölfle, Phys. Rev. Lett. **89**, 236402 (2002)
74. K. Haule, A. Rosch, J. Kroha, P. Wölfle, Phys. Rev. B **68**, 155119 (2003)
75. F. B. Anders, M. Jarrel, and D. Cox, Phys. Rev. Lett. **78**, 2000 (1997)
76. A. Schiller, F. B. Anders, and D. Cox, Phys. Rev. Lett. **81**, 3235 (1998)
77. M. Arnold and J. Kroha, Phys. Rev. Lett. **100**, 046404 (2008)
78. F. Reinert *et al.*, Phys. Rev. Lett. **87**, 106401 (2001)

79. D. Ehm *et al.*, Phys. Rev. B **76**, 045117 (2007)
80. D.L. Cox, A.R. Ruckenstein, Phys. Rev. Lett. **71**, 1613 (1993)
81. S. Kirchner and J. Kroha, J. Low Temp. Phys. **126**, 1233 (2002)
82. J.R. Schrieffer and P.A. Wolff, Phys. Rev. **149**, 491 (1966)
83. K. Haule, S. Kirchner, J. Kroha, and P. Wölfle: Phys. Rev. B **64**, 155111 (2001)
84. J. Holm, K. Schönhammer, Solid State Comm. **69**, 969 (1989)
85. O. Sakai, M. Motizuki, T. Kasuya, Springer Series in Solid-State Sciences **81**, 45 (Springer, 1988)
86. Th. Pruschke and N. Grewe, Z. Phys. B **74**, 439 (1989)
87. We are grateful to T. A. Costi for providing the NRG data.
88. F. B. Anders, N. Grewe: Europhys. Lett. **26**, (1994) 551.
89. J. Kroha and P. Wölfle, in **Theoretical Methods for Strongly Correlated Electrons**, CRM Series in Mathematical Physics, Springer, New York, pp 297 (2003)
90. S. Kirchner, J. Kroha, P. Wölfle: Phys. Rev. B **70** (2004) 165102.
91. H. Keiter and K. Baumgartner, Phys. Stat. Sol. (b) **242** (2), 377 (2005)
92. H. Keiter and K. Baumgartner, and S. Duffe, Phys. Stat. Sol. (b) **244** (7), 2357 (2007)
93. J. Kroha, P. Wölfle: unpublished.
94. Note, however, that CTMA includes all potential scattering terms up to $O(\Gamma^4)$.
95. P. W. Anderson, J. Phys. C **3**, 2439 (1970)
96. K. G. Wilson, Rev. Mod. Phys. **47**, 773 (1975)
97. D. Goldhaber-Gordon, et al., Nature (London) **391**, 156 (1998)
98. S. M. Cronenwett, T. H. Oosterkamp, and L. P. Kouwenhoven, Science **281**, 540 (1998)
99. A. Rosch, J. Paaske, J. Kroha, and P. Wölfle, Phys. Rev. Lett. **90**, 076804 (2003)
100. A. Rosch, J. Paaske, J. Kroha, and P. Wölfle, J. Phys. Soc. Japan **74**, 118 (2005)
101. J. Paaske, A. Rosch, and P. Wölfle, Phys. Rev. B **69**, 155330 (2004)
102. J. Paaske, A. Rosch, J. Kroha, and P. Wölfle, Phys. Rev. B **70**, 155301 (2004)
103. H. Schmidt and P. Wölfle, Ann. Phys. (Berlin) **19**, 60 (2010)
104. A. Rosch, J. Kroha, and P. Wölfle, Phys. Rev. Lett. **57**, 156802 (2003)
105. J. Paaske, A. Rosch, P. Wölfle, C. M. Marcus, and J. Nygård, Nature Physics **2**, 460 (2006)
106. V. Koerting, P. Wölfle, and J. Paaske, Phys. Rev. Lett. **99**, 036807 (2007)
107. V. Koerting, J. Paaske, and P. Wölfle, Phys. Rev. B **77**, 165122 (2008)
108. S. Schmaus, V. Koerting, J. Paaske, T. S. Jespersen, J. Nygård, and P. Wölfle, Phys. Rev. B **79**, 045105 (2009)
109. C.-H. Chung, G. Zarand, and P. Wölfle, Phys. Rev. **77**, 035120 (2008)
110. C.-H. Chung, K. LeHur, M. Vojta, and P. Wölfle, Phys. Rev. Lett. **102**, 216803 (2009)
111. U. Larsen and R. D. Mattuck, Proceedings of the International Conference on Magnetism, Moscow, U.S.S.R. 1973 (Nauka, Moscow) Vol5, p.88 (1974); U. Larsen, Phys. Lett. A **40**, 39 (1972)
112. J. Paaske, H. Schmidt, and P. Wölfle, to be published (2011)
113. M. Salmhofer, "Renormalization: An Introduction " (Springer, Berlin, 1998)
114. V. Meden, Advances in Solid State Physics, Vol. 46, edited by R. Haug (Springer, New York, 2007)
115. W. Metzner, Functional Renormalization Group Aapproach to Interacting Systems, in: Lecture Notes in Physics (Springer, Berlin, 2007)

116. A. A. Katanin, Phys. Rev. **70**, 115109 (2004)
117. J. Reuther, P. Wölfle, R. Darradi, W. Brenig, M. Arlego, and J. Richter, Phys. Rev. B **83**, 064416 (2011)

# Index

# List of Figures